UCLA
COMPUTATIONAL AND APPLIED MATHEMATICS

An Isobaric Fix for the Overheating Problem in Multimaterial Compressible Flows

Ronald P. Fedkiw
Antonio Marquina
Barry Merriman

February 1998

CAM Report 98-5

Department of Mathematics
University of California, Los Angeles
Los Angeles, CA. 90095-1555

An Isobaric Fix for the Overheating Problem in Multimaterial Compressible Flows

Ronald P. Fedkiw *
Antonio Marquina †
Barry Merriman *

September 30, 1998

Abstract

In many problems of interest, solid objects are treated as rigid bodies in compressible flowfields. When these solid objects interact with certain features of the compressible flowfield, inaccurate solutions may develop. In particular, the well known "overheating effect" occurs when a shock reflects off of a stationary solid wall boundary causing overshoots in temperature and density, while pressure and velocity remain constant (see e.g. [3, 7, 13, 14]). This "overheating effect" is more dramatic when compressible flows are coupled to moving solid objects (e.g. moving pistons), where the nonphysical density and temperature overshoots can be cumulative and lead to negative values.

We consider the general class of material interface problems where numerical methods can predict pressure and velocity adequately, but fail miserably in their prediction of density and temperature. Motivated by both total variation considerations and physical considerations, we have developed a simple but general boundary condition for this class of problems. This new boundary condition does not change the pressure or the velocity predicted by the numerical method, but does change the density and the temperature in a fashion consistent with the equation of state resulting in new values that minimize a specific measure of variation at the boundary.

*Research supported in part by ONR N00014-97-1-0027 and ONR N00014-97-1-0968
†Research supported in part by DGICYT PB94-0987 and NSF INT9602089

1 Introduction

The well known "overheating effect" occurs when a shock reflects off of a stationary solid wall boundary causing overshoots in temperature and density, while pressure and velocity remain constant. Note that the solid wall boundary condition is usually applied as a reflection condition so that a shock impinging on a wall is met by a reflected shock of equal strength traveling in the opposite direction causing the appropriate reflection. (This leads one to the obvious conclusion that "overheating" may occur within a fluid when two equal strength shocks collide.) In [7], Glaister illustrates "overheating effects" at solid wall boundaries for many different equations of state, including the standard gamma law gas.

In [13], Menikoff argues that this error is caused by the smeared out numerical shock profile and that the spatial width of this error shrinks to zero as the effective scheme viscosity shrinks to zero. However, he also shows that the maximum overshoot at the wall does not shrink as the numerical dissipation goes to zero, i.e. the solution converges in the L^2 sense, but not in the L^∞ sense as the scheme viscosity approaches zero. In addition, he points out that the pressure and velocity profiles at the wall equilibrate quickly, while the temperature and density (or equivalently entropy) errors persist. Menikoff believes that this error is a symptom of the numerical scheme's unsuccessful attempt to model a physical phenomenon which occurs in real shock tubes.

In [14], Noh had pointed out many of the effects that Menikoff later discussed in [13]. Noh also stated that heat conduction at the wall would dissipate this entropy error and that the failure of numerical schemes is due in part to the absence of heat conduction at the wall. In fact, he shows that a scheme with built in heat conduction could help to alleviate the problem, allowing convergence in the L^∞ sense as well.

In [3], Marquina proposed a flux splitting method which seems to possess a built in heat conduction mechanism. When this flux splitting is used with a low viscosity scheme (e.g. ENO [16] or WENO [10]), the error due to scheme viscosity is minimized and the built in heat conduction mechanism helps to dissipate the remaining entropy errors, allowing convergence in both the L^2 and L^∞ sense. In general this works well, but there are times when the heat conduction mechanism invoked by Marquina's flux splitting works on a

much slower time scale than the accumulation of the entropy error leading to a lack of convergence of the solution and the possibility of polluting other flow features in the computational domain.

Suppose we solve the Euler equations on a fixed grid with a moving solid object. The solid object will sweep through the compressible flow causing the appearance and disappearance of grid points in the Eulerian flow. For example, consider a piston moving from left to right in a one dimensional Eulerian code where the piston continues to cross over grid points removing them from the computational flowfield. In these types of problems, the entropy errors occurring at the interface will be cumulative and may accumulate faster than the built in heat conduction mechanism can dissipate them. In fact, this can lead to dramatic overshoots in the solution, resulting in negative values in density or temperature. In these instances one needs to fix the entropy error faster than it accumulates. One natural way of doing this is by the application of a boundary condition.

Consider the Euler equations at a given point. If we fix pressure and velocity, then there is one degree of freedom in choosing the solution, e.g. we may choose density, then the equation of state determines the temperature (and thus the internal energy). "Overheating" occurs, when the numerical method chooses a value from this one parameter family which is widely different from the accepted physical value. In these instances, pressure and velocity seem to match the accepted solution, but the scheme does not predict an acceptable value for the third variable (density or temperature). In the common instance that this "overheating" occurs at a material boundary, it usually starts locally, motivating the implementation of a *fix* in the form of a boundary condition.

We begin by assuming that the numerical scheme has chosen an adequate pressure and consider the problem from a physical standpoint. On a graph of temperature versus density, this pressure dictates the isobar (constant pressure line) that the solution to the problem lies on. For the case of an ideal gas, with equation of state $p = \rho RT$, the isobars are a family of hyperbolae of the form $T = \frac{A_o}{\rho}$ where $A_o = \frac{p_o}{R}$ is a different constant on each isobar (i.e. the hyperbolae are parameterized by pressure and a specific isobar can be labeled $p = p_o$). The pressure predicted by the numerical schemes dictates the choice of hyperbola associated with the solution. "Overheating" occurs when the numerical scheme chooses a density which is too small corresponding to a temperature which is too large. Similarly, "underheating" occurs when the numerical scheme chooses a density which is too large corresponding to a temperature which is too small. Since every point on this isobar has the

same pressure, we are free to choose any point we wish, without changing the pressure predicted by the numerical scheme. Our boundary condition consists of choosing a point on this isobar which is a better candidate for the solution than the obviously wrong choice given by the numerical scheme. That is, the numerical method picks out a reasonable isobar (i.e. pressure), but chooses the wrong point on that isobar. Our boundary condition consists of choosing a better point.

In the extreme limits of the hyperbola, we may choose density as large as we wish (small temperature) or as small as we wish (large temperature). Since both of these choices lead to extreme "overheating", and our goal is to reduce "overheating", we want to avoid the ends of the hyperbola and stay near the center. However, there is no clear choice for the point without some measure of an acceptable solution. Since we believe that "overheating" starts locally, near a material interface, we apply our "overheating fix" as a boundary condition and assume that the nearby points are better behaved (no "overheating" or less dramatic "overheating") using them as a reference from which to choose our boundary condition. We will choose our boundary condition on our fixed isobar (given by the numerical scheme) to minimize the difference in behavior between it and one or more of its neighbors.

2 Euler Equations

Consider the 1D Euler equations

$$\begin{pmatrix} \rho \\ \rho u \\ E \end{pmatrix}_t + \begin{pmatrix} \rho u \\ \rho u^2 + p \\ (E+p)u \end{pmatrix}_x = 0 \tag{1}$$

where t is time, x is space, ρ is the density, u is the velocity, E is the total energy per unit volume, and p is the pressure. The total energy is the sum of the internal energy and the kinetic energy,

$$E = \rho e + \frac{\rho u^2}{2} \tag{2}$$

where e is the internal energy per unit mass.

In general, the pressure can be written as a function of density and internal energy, $p = p(\rho, e)$, or as a function of density and temperature, $p = p(\rho, T)$. In order to complete the model, we need an expression for the internal energy per unit mass. Since $e = e(\rho, T)$ we write

$$de = \left(\frac{\partial e}{\partial \rho}\right)_T d\rho + \left(\frac{\partial e}{\partial T}\right)_\rho dT \tag{3}$$

which can be shown to be equivalent to

$$de = \left(\frac{p - T p_T}{\rho^2}\right) d\rho + c_v dT \tag{4}$$

where c_v is the specific heat at constant volume. [1]

The sound speeds associated with the equations depend on the partial derivatives of the pressure, either p_ρ and p_e or p_ρ and p_T, where the change of variables from density and internal energy to density and temperature is governed by the following relations

$$p_\rho \rightarrow p_\rho - \left(\frac{p - T p_T}{c_v \rho^2}\right) p_T \tag{5}$$

$$p_e \rightarrow \left(\frac{1}{c_v}\right) p_T \tag{6}$$

and the sound speed c is given by

$$c = \sqrt{p_\rho + \frac{pp_e}{\rho^2}} \tag{7}$$

for the case where $p = p(\rho, e)$ and

$$c = \sqrt{p_\rho + \frac{T(p_T)^2}{c_v \rho^2}} \tag{8}$$

for the case where $p = p(\rho, T)$.

3 Ideal Gas

We will motivate our new boundary condition by first considering an ideal gas. For an ideal gas $p = \rho RT$ where $R = \frac{R_u}{M}$ is the specific gas constant, with $R_u \approx 8.31451 \frac{J}{molK}$ the universal gas constant and M the molecular weight of the gas. Also valid for an ideal gas is $c_p - c_v = R$ where c_p is the specific heat at constant pressure. Additionally, gamma as the ratio of specific heats $\gamma = \frac{c_p}{c_v}$. [6]

For an ideal gas, equation 4 becomes

$$de = c_v dT \tag{9}$$

and assuming that c_v does not depend on temperature (calorically perfect gas), we integrate to obtain

$$e = c_v T \tag{10}$$

where we have set e to be zero at $0K$. Note that e is not uniquely determined, and we could choose any value for e at $0K$ (although one needs to use caution when dealing with more than one material to be sure that integration constants are consistent with the heat release in any chemical reactions that occur).

Suppose that we have acceptable reference values for all conserved variables from which we can assemble $\hat{p}$, $\hat{\rho}$, and $\hat{T}$. Also suppose that somewhere "nearby" the reference values, we have values for the conserved variables with an acceptable pressure, p_o, but unacceptable values for the density, ρ_o, and temperature, T_o. We wish to choose new values for the density and temperature from the one parameter family which lies on the isobar $p = p_o$. Since the reference state is "nearby", we will use those values to help us determine the new density and temperature.

First consider the case where $p_o = \hat{p}$, where the reference point and the point where we wish to apply our boundary condition both lie on the same isobar. In this case, we want the points to coincide, i.e. choose $\rho_o = \hat{\rho}$ and $T_o = \hat{T}$. For this choice, all measures of variation are zero since the values are identical. Note that any other choice on this isobar gives a splitting of the density and temperature, i.e. density increases (decreases) while temperature decreases (increases). This splitting is the essence of "overheating", and it is

this splitting behavior that we wish to avoid. We can avoid this by imposing a simple restriction, that an increase in pressure should give an increase in both density and temperature, while a decrease in pressure should give a decrease in both density and temperature. We illustrate this graphically in figure 1. The lines $\rho = \hat{\rho}$ and $T = \hat{T}$ divide the temperature versus density graph of isobars into four regions based on the reference value. For $p_o > \hat{p}$ the solution must lie in the upper right corner, while $p_o < \hat{p}$ dictates that the solution must lie in the lower left corner. The diagonal corners represent splitting, where an increase (or decrease) in pressure is achieved by splitting density and temperature. Note that this splitting always gives a solution with more variation. For example, an increase in pressure can be achieved by increasing density, or temperature, or both. But if one of these decreases (density or temperature), then the other must increase just to balance out this decrease and achieve the same pressure, and then increase even more to match the pressure rise. Thus the balancing (or splitting) to achieve the same pressure is wasted variation, and only the final increase to achieve the necessary pressure increase is needed variation.

3.1 Some Measures of Variation

Given a reference state $(\hat{\rho}, \hat{T})$, we measure the variation from it by,

$$V = \frac{|\rho - \hat{\rho}|}{\hat{\rho}} + \frac{|T - \hat{T}|}{\hat{T}} \tag{11}$$

where the division by $\hat{\rho}$ and $\hat{T}$ is done to nondimensionalize the individual variations of density and temperature to give them equal weight. If ρ and T lie on a fixed isobar, chosen by the numerical scheme, then V is a function of one variable, since specifying ρ fixes T and vice versa. We differentiate V as a function of ρ (differentiating as a function of T leads to the same result) to get

$$V'(\rho) = \frac{S(\rho - \hat{\rho})}{\hat{\rho}} + \frac{S(T - \hat{T})T'(\rho)}{\hat{T}} \tag{12}$$

where S is the sign function. (Note that the expression is not valid when $\rho = \hat{\rho}$ or $T = \hat{T}$). Next we enforce the condition that there is no splitting, meaning that ρ and T both increase for an increase in pressure and both decrease for a decrease in pressure. This condition implies that $S(\rho - \hat{\rho}) =$

$S(T-\hat{T})$, so that setting $V'(\rho) = 0$ allows us to divide out the sign functions getting

$$T'(\rho) = -\frac{\hat{T}}{\hat{\rho}} \tag{13}$$

where $T'(\rho)$ is evaluated at some fixed pressure p_o. For an ideal gas

$$T'(\rho) = -\frac{p_o}{\rho^2 R} = -\frac{\rho R T}{\rho^2 R} = -\frac{T}{\rho} \tag{14}$$

leading to the condition that

$$-\frac{T}{\rho} = -\frac{\hat{T}}{\hat{\rho}} \tag{15}$$

which can be rewritten using the equation of state to obtain

$$\rho = \hat{\rho}\sqrt{\frac{p_o}{\hat{p}}} \tag{16}$$

as an exact closed form solution for the density. Or we could write equation 16 as

$$T = \hat{T}\sqrt{\frac{p_o}{\hat{p}}} \tag{17}$$

giving an exact closed form solution for the temperature. Notice how an increase in pressure, $p_o > \hat{p}$, leads to an increase in both density and temperature, while a decrease in pressure, $p_o < \hat{p}$, leads to a decrease in both density and temperature. In addition, note that these closed form solutions predict equality in density and temperature when we have equality in pressure, $p_o = \hat{p}$, implying that they are valid in all cases.

We take a second derivative of equation 11 to get

$$V''(\rho) = \frac{S(T-\hat{T})T''(\rho)}{\hat{T}} \tag{18}$$

which is not valid when $\rho = \hat{\rho}$ or $T = \hat{T}$. For an ideal gas, $T''(\rho) > 0$. This implies that our closed form solution in equation 16 gives the minimum value for V in the case of $p_o > \hat{p}$ where $S(T-\hat{T}) > 0$, but gives the maximum value of V in the case of $p_o < \hat{p}$ where $S(T-\hat{T}) < 0$. In fact, the minimum value for V occurs on the boundary of the nonsplitting region in case of $p_o < \hat{p}$.

Figure 2 is a graph of the minimization of V under the no splitting restriction. Notice that the solution is unique for $p_o \geq \hat{p}$ and is given by equation 16. Then for $p_o < \hat{p}$, the solution splits into two pieces and becomes multivalued with $\rho = \hat{\rho}$ or $T = \hat{T}$ giving the minimization in the nonsplitting region.

At this point, we make two notes, concerning the case where $p_o < \hat{p}$. First there is no clear reason to choose $\rho = \hat{\rho}$ instead of $T = \hat{T}$ or vice versa. Second, both of these solutions border on the splitting region leading to the possibility that small variations in the choice of ρ and T may lead to "overheating".

Next consider equation 13 which dictates that the point chosen on the isobar $p = p_o$ to fix "overheating" will have a slope of $-\frac{\hat{T}}{\hat{\rho}}$. In addition note that the reference point, $(\hat{\rho}, \hat{T})$, on the isobar $p = \hat{p}$ also has slope $-\frac{\hat{T}}{\hat{\rho}}$, which can be see by evaluating $T'(\rho)$ at $(\hat{\rho}, \hat{T})$. Thus equation 13 says that the point chosen on the isobar $p = p_o$ should have the same slope, $T'(\rho)$, as the reference point on the isobar $p = \hat{p}$. We could think of this as minimizing the variation in behavior between the two points, i.e. we could minimize the difference between the slopes and arrive at equation 16 as our solution. This especially makes sense when one considers that

$$T'(\rho) = -\frac{p_\rho}{p_T} \tag{19}$$

and considers the important role that p_ρ and p_T play in the sound speeds. Figure 3 shows the solution given by minimizing the variation in behavior as defined by the slope of the isobar at the given point.

Consider the alternative formulation of the pressure as $p = p(\rho, e)$. For a calorically perfect ideal gas $e = c_v T$ and so $e'(\rho) = c_v T'(\rho)$ and thus minimizing the variation in behavior based on $T'(\rho)$ is equivalent to minimizing the variation in behavior based on $e'(\rho)$ leading to the solution in figure 3 and equation 16. However, this is not true for general equations of state where minimizing the variation in behavior based on $e'(\rho)$ may be different than minimizing the variation in behavior based on $T'(\rho)$. In addition, note that $e = c_v T$ implies that the measure of variation in equation 11 is identical if we consider ρ and e instead of ρ and T with the result shown in figure 2. Again, this is only valid when $e = c_v T$ with c_v constant.

Since the errors in density and temperature can be seen in the entropy of an ideal gas defined by

$$S = \frac{p}{\rho^\gamma} \tag{20}$$

it is natural to analyze the solution that occurs if we attempt to minimize the variation in entropy. In [17], Woodward and Colella compute a flow past a corner problem and show that the traditional methods do not give the appropriate steady state solution. They notice a large entropy gradient at the corner and fix it by enforcing constant entropy. This entropy fix removes the boundary layer in entropy, but the solution still does not converge to a steady state. An additional constant enthalpy fix is applied to get the solution to converge to a steady state. This is an extremely popular method and more current details can be seen in [15, 3]. We note that the constant entropy and enthalpy fix is only valid on a streamline, and that Woodward and Colella use an upstream point as their reference point. In general, one cannot always find an upstream reference point and this fix cannot be applied. In fact, the constant enthalpy fix will change the velocity field which is unwanted in many cases. Note that this fix is isobaric (it does not change the pressure).

From a more general standpoint we dismiss the use of a constant enthalpy fix, but consider a constant entropy fix. The constant entropy solution, or the minimization of the variation in entropy, is shown in figure 4. While it lies in the nonsplitting region, we note that it makes the assumption that the points lie on the same streamline which is not necessarily true.

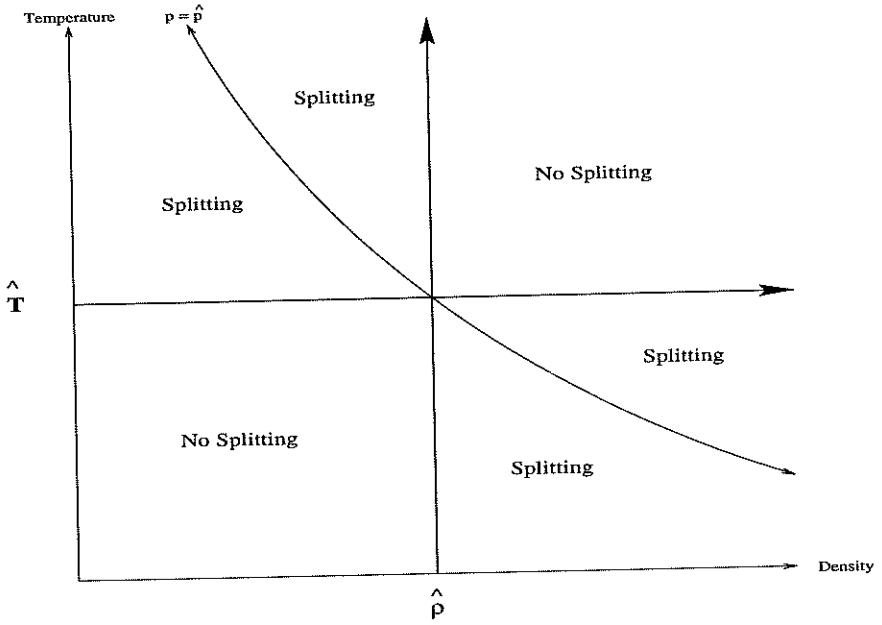

Figure 1: Diagram of "overheating" regions

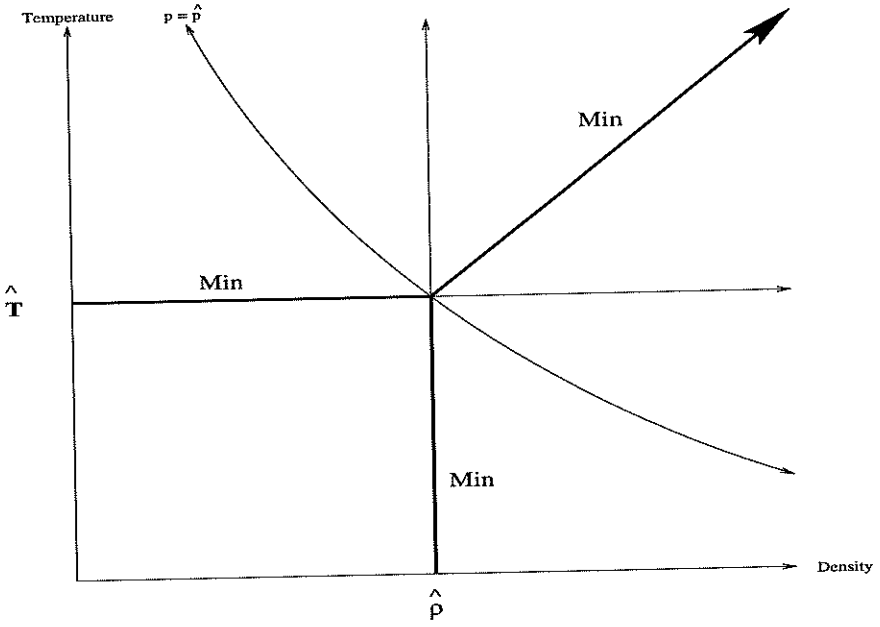

Figure 2: Minimization of the variation V

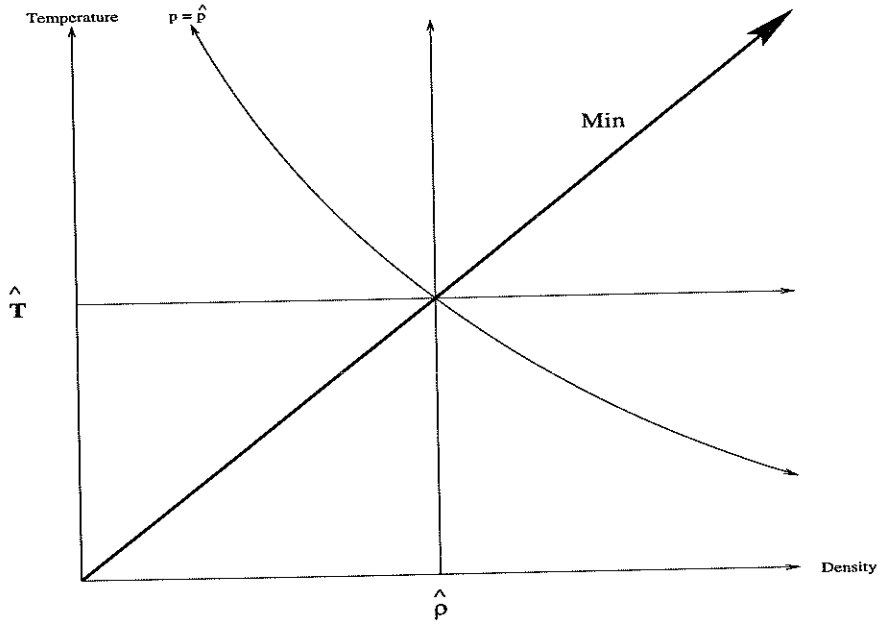

Figure 3: Minimization of the variation in slope $T'(\rho)$

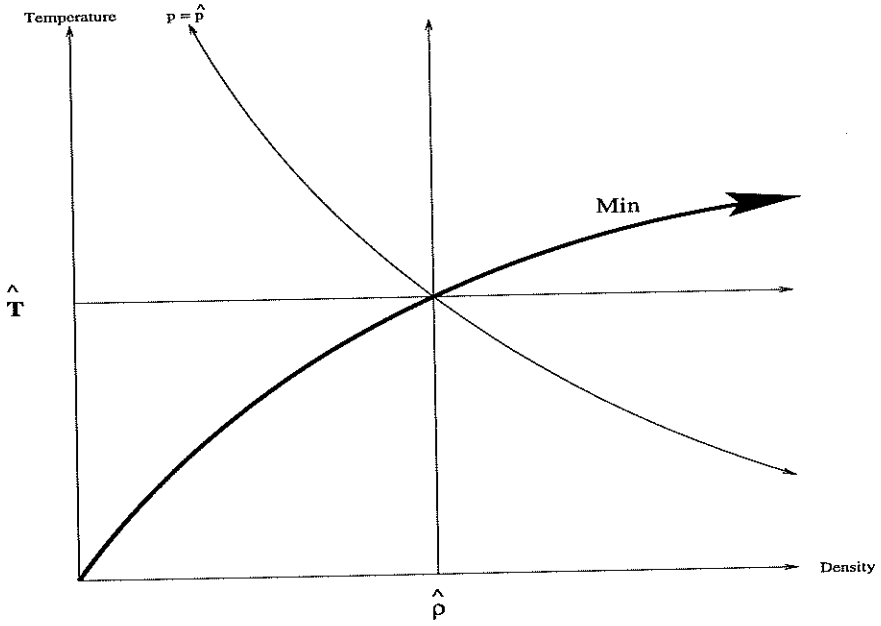

Figure 4: Minimization of the variation in entropy S

4 Isobaric Fix

Given a reference state $(\hat{\rho}, \hat{T})$ on an isobar $p = \hat{p}$, we need to choose a value for (ρ, T) on the isobar $p = p_o$ in order to minimize some sense of the variation to avoid "overheating". While there seem to be a few ways of doing this, we will focus our attention on three specific ways: constant $T'(\rho)$, constant $e'(\rho)$, or constant S. For an ideal gas, holding either $T'(\rho)$ or $e'(\rho)$ constant leads to equation 16, while holding entropy constant leads to

$$\rho = \hat{\rho} \left(\frac{p_o}{\hat{p}} \right)^{\frac{1}{\gamma}} \tag{21}$$

as our isobaric fix.

For general equations of state, if we hold

$$T'(\rho) = -\frac{p_\rho}{p_T} \tag{22}$$

constant, than we need some assumptions to guarantee that the solution exists. For example, if fixed pressures have $T'(\rho) < 0$ with $\lim_{\rho \to 0} T(\rho) = \infty$ and $\lim_{\rho \to \infty} T(\rho) = 0$ (to establish the asymptotes), than a solution exists. In addition, $T''(\rho) > 0$ will guarantee uniqueness. If we hold

$$e'(\rho) = -\frac{p_\rho}{p_e} \tag{23}$$

constant, than we need similar conditions on $e(\rho)$ to those mentioned above for $T(\rho)$ in order to guarantee a unique solution.

For the general constant entropy case, note that entropy has partial derivatives orthogonal to the left eigenvectors of the truly nonlinear fields, implying that they are a multiple of the left eigenvector of the linearly degenerate field. For the one dimensional Euler equations, we have [5]

$$\begin{pmatrix} S_\rho \\ S_{\rho u} \\ S_E \end{pmatrix} = \alpha \begin{pmatrix} \frac{E+p}{\rho} - u^2 \\ u \\ -1 \end{pmatrix} \tag{24}$$

where α is a constant and can be seen to be equal to $-S_E$ from the above equation. We make a change of variables from the conserved variables ρ, ρu,

and E to the new variables ρ, u, and e giving the following relations

$$S_\rho \to S_\rho - \left(\frac{u}{\rho}\right) S_u + \left(\frac{u^2}{2\rho} - \frac{e}{\rho}\right) S_e \tag{25}$$

$$S_{\rho u} \to \left(\frac{1}{\rho}\right) S_u - \left(\frac{u}{\rho}\right) S_e \tag{26}$$

$$S_E \to \left(\frac{1}{\rho}\right) S_E \tag{27}$$

which can be substituted into equation 24, while setting $\alpha = -S_E$ and $S_u = 0$ to get the relation

$$S_\rho = -\left(\frac{p}{\rho^2}\right) S_e \tag{28}$$

for entropy. Since we only care about constant entropy, we write

$$dS = \left(\frac{\partial S}{\partial \rho}\right)_e d\rho + \left(\frac{\partial S}{\partial e}\right)_\rho de = 0 \tag{29}$$

which can be rearranged to get

$$\frac{de}{d\rho} = \frac{S_\rho}{S_e} \tag{30}$$

and using equation 28, we have

$$\frac{de}{d\rho} = \frac{p}{\rho^2} \tag{31}$$

as an equation that guarantees constant entropy.

As an example, consider a somewhat general equation of state

$$p = f(\rho) + g(\rho)e \tag{32}$$

where $f(\rho)$ and $g(\rho)$ are arbitrary functions of ρ. Then using equation 31 to impose constant entropy, we have

$$\frac{de}{d\rho} - \left(\frac{g(\rho)}{\rho^2}\right) e = \frac{f(\rho)}{\rho^2} \tag{33}$$

which is a first order linear differential equation, solved with the integrating factor

$$\mu = \exp\left(-\int \frac{g(\rho)}{\rho^2} d\rho\right) \tag{34}$$

yielding the solution

$$e = \frac{1}{\mu}\left[\int \frac{\mu f(\rho)}{\rho^2} d\rho + C(S)\right] \tag{35}$$

where $C(S)$ is a constant function of S. For an ideal gas, $p = (\gamma - 1)\rho e$ with $f(\rho) = 0$ and $g(\rho) = (\gamma - 1)\rho$ giving $e = C(S)\rho^{\gamma-1}$ from equation 35. We solve for $C(S)$ using the equation of state to get

$$C(S) = \frac{p}{(\gamma - 1)\rho^{\gamma}} \tag{36}$$

or equivalently

$$\hat{C}(S) = \frac{p}{\rho^{\gamma}} \tag{37}$$

leading to

$$\rho = \hat{\rho}\left(\frac{p_o}{\hat{p}}\right)^{\frac{1}{\gamma}} \tag{38}$$

as a closed form solution (which is very similar to equation 16).

4.1 Example: Tait Solid

Consider the Tait equation of state for a solid given by

$$p = (\gamma - 1)c_v \rho T - \frac{\rho_a \sigma}{\gamma} \tag{39}$$

where γ, c_v, ρ_a, and σ are the Tait parameter, specific heat at constant volume, initial ambient density, and the nonideal solid parameter respectively [8]. We integrate equation 4, setting the integration constant to q which is the chemical energy stored in the solid,

$$e = \frac{\rho_a \sigma}{\gamma \rho} + c_v T + q \tag{40}$$

Since $T'(\rho) < 0$, $\lim_{\rho \to 0} T(\rho) = \infty$, $\lim_{\rho \to \infty} T(\rho) = 0$ and $T''(\rho) > 0$, there is a unique solution for the $T'(\rho)$ constant isobaric fix. We evaluate equation 22 to get

$$T'(\rho) = -\frac{T}{\rho} \tag{41}$$

which leads to the condition

$$-\frac{T}{\rho} = -\frac{\hat{T}}{\hat{\rho}} \tag{42}$$

that can be rewritten using the equation of state as

$$\rho = \hat{\rho}\sqrt{\frac{p_o + \frac{\rho_a \sigma}{\gamma}}{\hat{p} + \frac{\rho_a \sigma}{\gamma}}} \tag{43}$$

or equivalently

$$T = \hat{T}\sqrt{\frac{p_o + \frac{\rho_a \sigma}{\gamma}}{\hat{p} + \frac{\rho_a \sigma}{\gamma}}} \tag{44}$$

giving an exact closed form solution.

Since $e'(\rho) < 0$, $\lim_{\rho \to 0} e(\rho) = \infty$, $\lim_{\rho \to \infty} e(\rho) = q$ and $e''(\rho) > 0$ there is a unique solution for the $e'(\rho)$ constant isobaric fix. Note that the horizontal asymptote $e = q$ is sufficient for our purposes. We evaluate equation 23 to get

$$e'(\rho) = -\frac{(e - q)}{\rho} \tag{45}$$

which leads to the condition

$$-\frac{(e - q)}{\rho} = -\frac{(\hat{e} - q)}{\hat{\rho}} \tag{46}$$

that can be rewritten using the equation of state as

$$\rho = \hat{\rho}\sqrt{\frac{p_o + \rho_a \sigma}{\hat{p} + \rho_a \sigma}} \tag{47}$$

or equivalently

$$e - q = (\hat{e} - q)\sqrt{\frac{p_o + \rho_a \sigma}{\hat{p} + \rho_a \sigma}} \tag{48}$$

giving an exact closed form solution different from equations 43 and 44.

For constant entropy, we combine equations 39 and 40 to get

$$p = (\gamma - 1)\rho(e - q) - \rho_a\sigma \tag{49}$$

with $f(\rho) = -(\gamma - 1)\rho q - \rho_a\sigma$ and $g(\rho) = (\gamma - 1)\rho$ implying that the integrating factor in equation 34 is $\mu = \rho^{1-\gamma}$ and the solution in equation 35 is

$$C(S) = \frac{p + \frac{\rho_a\sigma}{\gamma}}{(\gamma - 1)\rho^\gamma} \tag{50}$$

after suitable application of the equation of state. We prefer the equivalent

$$\hat{C}(S) = \frac{p + \frac{\rho_a\sigma}{\gamma}}{\rho^\gamma} \tag{51}$$

as a more conventional definition. Note that this leads to

$$\rho = \hat{\rho}\left(\frac{p_o + \frac{\rho_a\sigma}{\gamma}}{\hat{p} + \frac{\rho_a\sigma}{\gamma}}\right)^{\frac{1}{\gamma}} \tag{52}$$

as a closed form solution which is more similar to equation 43 than to equation 47.

4.2 Example: Virial Gas

Consider the virial equation of state for a gas with the third and higher virial coefficients set to zero,

$$p = \rho RT(1 + b\rho) \tag{53}$$

where b is the second virial coefficient [1]. We integrate equation 4, setting the integration constant to zero, getting

$$e = c_v T \tag{54}$$

as our internal energy per unit mass.

Since $T'(\rho) < 0$, $\lim_{\rho\to 0} T(\rho) = \infty$, $\lim_{\rho\to\infty} T(\rho) = 0$ and $T''(\rho) > 0$ there is a unique solution for the $T'(\rho)$ constant isobaric fix. We evaluate equation 22 to get

$$T'(\rho) = -\frac{T(1 + 2b\rho)}{\rho(1 + b\rho)} \tag{55}$$

which leads to the condition

$$-\frac{T(1+2b\rho)}{\rho(1+b\rho)} = -\frac{\hat{T}(1+2b\hat{\rho})}{\hat{\rho}(1+b\hat{\rho})} = K \tag{56}$$

where K is a constant equal to $T'(\rho)$ evaluated at $(\hat{\rho}, \hat{T})$ on the isobar $p = \hat{p}$. We use the equation of state to rewrite this as

$$f(T) = T^4 + \left(\frac{4bp_o}{R}\right)T^3 - \left(\frac{p_o K}{R}\right)^2 = 0 \tag{57}$$

and use Newton Raphson iteration [2] of the form

$$T^{n+1} = T^n - \frac{f(T^n)}{f'(T^n)} \tag{58}$$

where

$$f'(T) = 4T^3 + \left(\frac{12bp_o}{R}\right)T^2 > 0 \tag{59}$$

with initial guess equal to either the reference temperature, $\hat{T}$, the temperature provided by the numerical scheme, T_o, or any other convenient guess. We could have approached this rootfinding through the density, but we have found that temperature iteration is easy to monitor and control [6].

Since $e'(\rho) < 0$, $\lim_{\rho\to 0} e(\rho) = \infty$, $\lim_{\rho\to\infty} e(\rho) = 0$ and $e''(\rho) > 0$ there is a unique solution for the $e'(\rho)$ constant isobaric fix. We evaluate equation 23 to get

$$e'(\rho) = -\frac{e(1+2b\rho)}{\rho(1+b\rho)} \tag{60}$$

which leads to the condition

$$-\frac{e(1+2b\rho)}{\rho(1+b\rho)} = -\frac{\hat{e}(1+2b\hat{\rho})}{\rho(1+b\hat{\rho})} \tag{61}$$

which can be rewritten to be identical to 56.

For constant entropy, we combine equations 53 and 54 to get

$$p = \left(\frac{R}{c_v}\right)\rho e(1+b\rho) \tag{62}$$

with $f(\rho) = 0$ and

$$g(\rho) = \left(\frac{R}{c_v}\right) \rho(1 + b\rho) \tag{63}$$

implying that the integrating factor in equation 34 is

$$\mu = \frac{1}{\rho^{\frac{R}{c_v}} \exp\left(\frac{bR\rho}{c_v}\right)} \tag{64}$$

and the solution in equation 35 is

$$C(S) = \frac{p}{\left(\frac{R}{c_v}\right)(1 + b\rho)\rho^{\frac{R}{c_v}+1} \exp\left(\frac{bR\rho}{c_v}\right)} \tag{65}$$

after suitable application of the equation of state. Once again we prefer

$$\hat{C}(S) = \frac{p}{(1 + b\rho)\rho^{\frac{R}{c_v}+1} \exp\left(\frac{bR\rho}{c_v}\right)} \tag{66}$$

as a more conventional definition. Note that setting $\frac{R}{c_v} = \gamma - 1$ and $b = 0$ reduces this to the ideal gas case as it should.

4.3 Which Isobaric Fix?

In general, our preference is to use the isobaric fix that works the best out of those that we find convenient to apply.

The constant entropy isobaric fix is difficult to write down in closed form for many general equations of state, and once written down not always easy to apply (e.g. consider the constant entropy isobaric fix for the virial gas above). In the case where the constant entropy isobaric fix is hard to derive and apply, we choose to consider either $T'(\rho)$ constant or $e'(\rho)$ constant or both, but ignore the constant entropy isobaric fix.

Sometimes, for equations of state of the form $p = p(\rho, T)$, with the entire problem formulated in terms of T, it may be difficult or just inconvenient to find relations with e. In these cases, we use the $T'(\rho)$ constant isobaric fix and ignore the $e'(\rho)$ constant isobaric fix. Likewise, equations of state of the form $p = p(\rho, e)$ with the entire problem formulated in terms of e, may not have readily available formulas based on T, so we only apply the $e'(\rho)$ constant isobaric fix, ignoring the $T'(\rho)$ constant isobaric fix.

For some equations of state, all analytic methods may be difficult or impossible to apply, e.g. consider an equation of state in tabular form. In these cases we advocate the use of the constant entropy isobaric fix, since a purely numerical approach is available. That is, given $\hat{p}$ and $\hat{\rho}$ at a suitable reference state along with p_o at the point in question, one can integrate an ordinary differential equation to find an appropriate density. At constant entropy,

$$\frac{dp}{d\rho} = c^2 \tag{67}$$

where c is the local speed of sound dependent on the local density and pressure (and partial derivatives of the pressure). We apply the constant entropy isobaric fix by integrating the ordinary differential equation

$$\frac{d\rho}{dp} = \frac{1}{c^2} \tag{68}$$

from $\hat{p}$ to p_o with initial data $\rho = \hat{\rho}$. The final value of ρ at $p = p_o$ is the value we use for the isobaric fix. Note that exact integration of this ordinary differential equation gives the same density as analytically applying the constant entropy isobaric fix. Our experience has shown that this numerical approach is fairly robust and easy to apply.

5 A Moving Piston

One way of simulating moving pistons is to transform the Euler equations to an accelerating reference frame which would keep the piston surface fixed in space and allow the use of exact ghost cells for a solid wall boundary condition. This transformation adds source terms to the right hand side of the momentum and energy equations which can be integrated in time along with the spatial derivative terms. The details are outlined in [8]. A drawback of this method is that it cannot conveniently treat multiple bodies with different accelerations at the same time. Since we wish to couple our Eulerian code to multiple moving objects and possibly to Lagrangian codes, we prefer to use the standard (non-transformed) Euler equations and treat the piston as a moving body with the appropriate boundary conditions. For a general discussion on boundary conditions, see chapter 19 in [9].

5.1 Ghost Cells

We will allow a piston to move across the domain from left to right, with a specific velocity. This will be accomplished by tracking the piston location (using a level set in 2D), and then using ghost cells to define the interior of the piston. For a piston moving with speed v_p, and exterior values of ρ, u, e, and E, we define the interior reflected values as

$$\rho_p = \rho, \qquad e_p = e \tag{69}$$

$$u_p = 2v_p - u, \qquad E_p = \rho e + \frac{\rho(2v_p - u)^2}{2} \tag{70}$$

For example, we consider a $20cm$ domain consisting of 200 grid cells, where the piston starts at rest at the left edge of the domain and moves with velocity $v_p(t)$. We compute this problem by setting the left hand boundary to $-.5cm$ instead of $0cm$, thus putting 5 ghost cells in our piston and increasing the total number of cells to 205.

5.2 Numerical Interpolation

Assume that a piston starts at $x = 0$ and that we have added y units of ghost cells to the left of $x = 0$. Consider the piston sitting at a point x_0 in space with a velocity v_p. Then the grid cells which lie inside the piston are numbered from 1 to i_0 where

$$i_0 = \left[\frac{y + x_0}{dx}\right] + 1 \tag{71}$$

where $[A]$ is the greatest integer less than or equal to A.

For each of the grid points i, from 1 to i_0, we identify the associated set of conserved variables located outside the piston. A grid point i is located at $x = (i-1)dx - y$ and so it is a distance $x_0 - (i-1)dx + y$ inside the piston surface, implying that the associated reflected point is at the location

$$\hat{x} = x_0 + x_0 - (i-1)dx + y \tag{72}$$

which has neighbors which are the grid nodes

$$j = \left[\frac{\hat{x} + y}{dx}\right] + 1 \tag{73}$$

and $j + 1$. The point is located

$$\epsilon = \hat{x} + y - (j-1)dx \tag{74}$$

units to the right of j and $dx - \epsilon$ units to the left of $j + 1$.

We will use a second order linear interpolation to find the values of the conserved variables, $\vec{U}$ in between the grid nodes. This is a second order boundary condition, and should be good enough for third order methods in the interior. If both j and $j + 1$ are exterior points, then the interpolated value for the conserved variables is,

$$\vec{U} = \vec{U}_j + \epsilon\left(\frac{\vec{U}_{j+1} - \vec{U}_j}{dx}\right) \tag{75}$$

otherwise if j is a point which is inside the piston, i.e. $j \leq i_0$, then

$$\vec{U} = \vec{U}_{j+1} + (dx - \epsilon)\left(\frac{\vec{U}_{j+1} - \vec{U}_{j+2}}{dx}\right) \tag{76}$$

using linear extrapolation from $\vec{U}_{j+1}$ and $\vec{U}_{j+2}$. Once the exact values of $\vec{U}$ are known, then the new interior values are defined above, based on the piston velocity, v_p.

6 Examples

For the ideal gas we consider air with $M = .029\frac{kg}{mol}$ and $\gamma = 1.4$. For the Tait solid equation of state, we have $\gamma = 5$, $c_v = 1,500\frac{J}{kgK}$, $\rho_a = 1,900\frac{kg}{m^3}$, $\sigma = 8,980,000\frac{m^2}{s^2}$, and $q = 0$. For the virial gas equation of state, we have $R = 286.7\frac{J}{kgK}$, $c_v = 716.8\frac{J}{kgK}$, and $b = .00076\frac{m^3}{kg}$.

The grid is set up to be a $1m$ domain with 200 cells. The piston (or wall if not moving) is located at the left hand side of the figure in all cases and ghost cells are added to the left of the piston. We do not print out the values of data at ghost cells, since they can be inferred from the real data points.

All schemes use 3rd order TVD Runge Kutta for the time stepping [16], and in each case the CFL is chosen near it's limit.

As specified earlier, the isobaric fix is applied as a boundary condition after each Euler substep of the TVD Runge Kutta method. That is, we update the conserved variables in the usual fashion for one substep, and then we use the isobaric fix to modify the computed values of the conserved variables near the wall. For example, suppose that the values of density, velocity, and pressure are ρ_1, u_1, and p_1 adjacent to the wall and ρ_2, u_2, and p_2 at the next point over which we will use as a reference point. Then in the case of an ideal gas, we can use equation 16 to define

$$\rho_{new} = \rho_2 \sqrt{\frac{p_1}{p_2}} \tag{77}$$

as the new density adjacent to the wall. Then ρ_{new}, u_1, and p_1 can be reassembled to get the new conserved variables.

6.1 Example 1

The purpose of this example is to illustrate how the isobaric fix works for a standard shock reflection problem. We generate a shock using a standard shock tube problem. The generated shock moves to the left until it intersects the solid wall (located at $0m$) and reflects off, causing "overheating". Note that we numerically cut off (and discard) the contact discontinuity and rarefaction so that they do not interfere with our reflected shock.

We use the ideal gas equation of state where the initial data for the shock tube problem has $u = 0$ and $T = 300K$. In addition, we choose the density to be $10\frac{kg}{m^3}$ on the left and $100\frac{kg}{m^3}$ on the right.

We use 3rd order ENO-RF [16] which is a low viscosity scheme and show the results in figure 5. Note the "overheating" errors in the temperature and the density. Figures 6 and 7 show the positive effect that the isobaric fix can have on these "overheating" errors. As shown in figure 8, the Marquina style Jacobian evaluation [3, 4] will also reduce overheating with its built in heat conduction mechanism (Note that ENO-LLF-M stands for ENO-LLF with the Marquina style Jacobian evaluation.) In figures 9 and 10, we show how the isobaric fix works in conjunction with the Marquina style Jacobian evaluation. Note that the isobaric fix did not affect the shock speed or strength. In fact the intermediate points inside the shock are almost in the same location.

At this point, we comment on conservation. A stationary solid wall boundary has a physical flux given by

$$\begin{pmatrix} \rho u \\ \rho u^2 + p \\ (E+p)u \end{pmatrix} = \begin{pmatrix} 0 \\ p \\ 0 \end{pmatrix} \tag{78}$$

since the velocity is identically zero. Thus, mass and energy are completely conserved while momentum is not conserved. The change in momentum for the computational domain can be found by summing the momentum fluxes at the boundaries. Achieving exact conservation for mass and energy can easily be accomplished for stationary walls aligned with the grid by setting the appropriate fluxes to zero. However, this can be excessively complicated to apply for multiple moving boundaries with irregular shapes. In either case, the isobaric fix will create a small conservation error in mass and energy in favor of a better solution. However, in the later case, difficulties of scheme implementation may force relaxation of mass and energy conservation even without the isobaric fix. In this case, the small conservation error generated by the isobaric fix is not an issue. Note that all the shocks in our examples are located in the correct cell and move with the appropriate speed, even with the relaxation of exact conservation at the boundary.

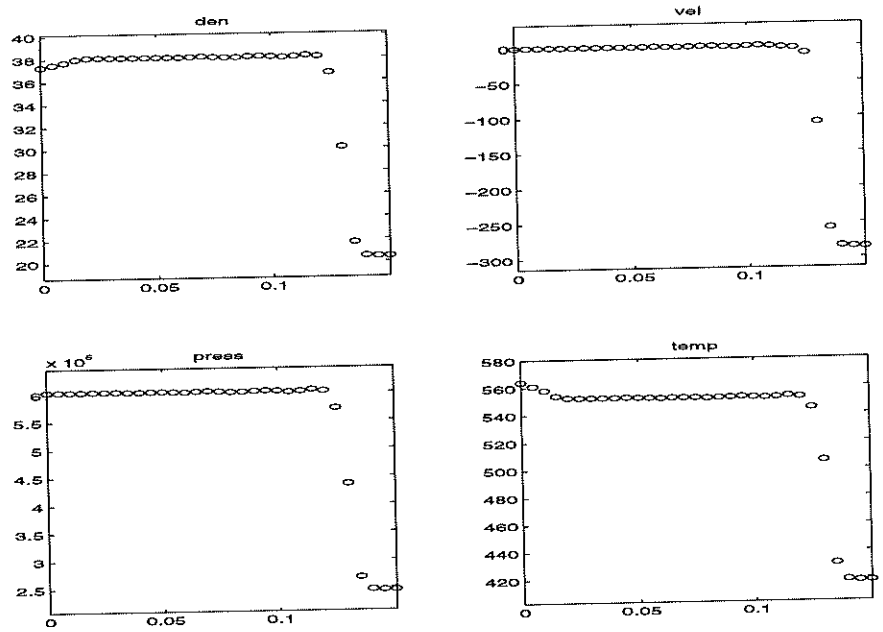

Figure 5: Ideal Gas, ENO-RF, "overheating"

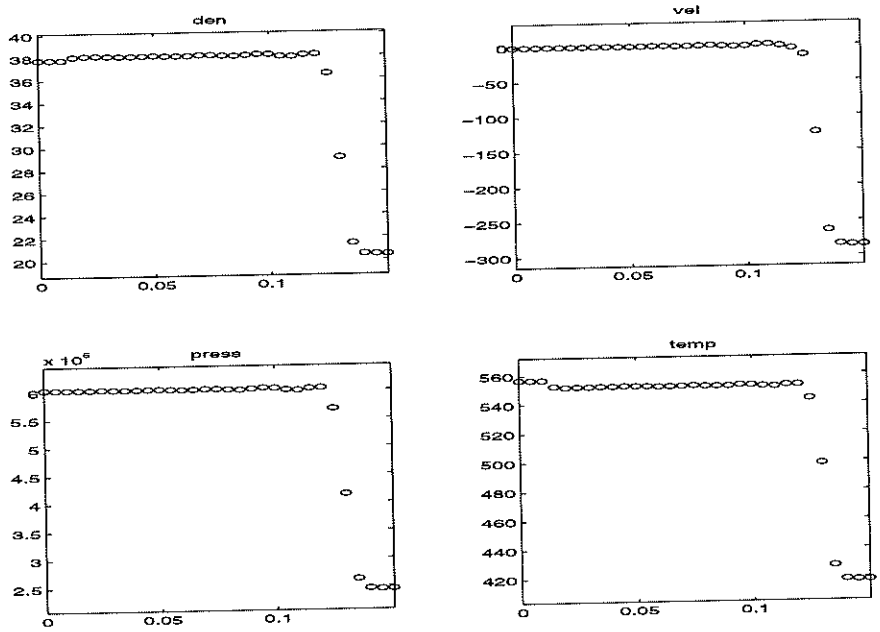

Figure 6: Ideal Gas, ENO-RF, $T'(\rho)$ constant

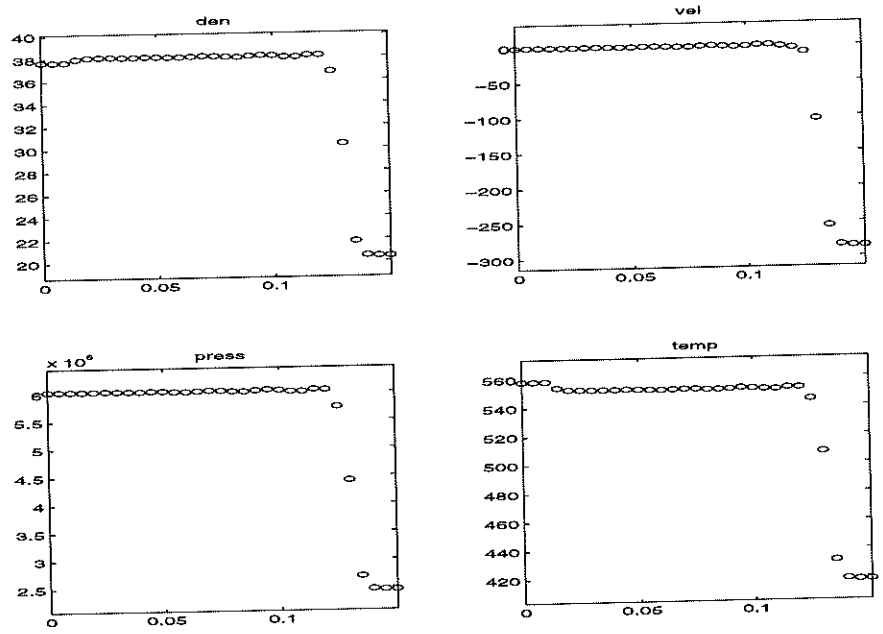

Figure 7: Ideal Gas, ENO-RF, constant entropy

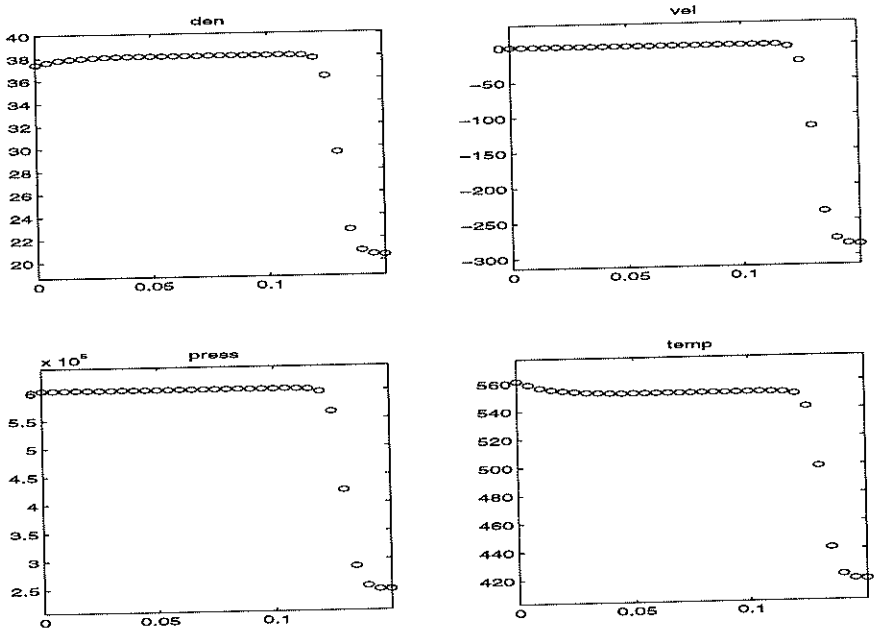

Figure 8: Ideal Gas, ENO-LLF-M

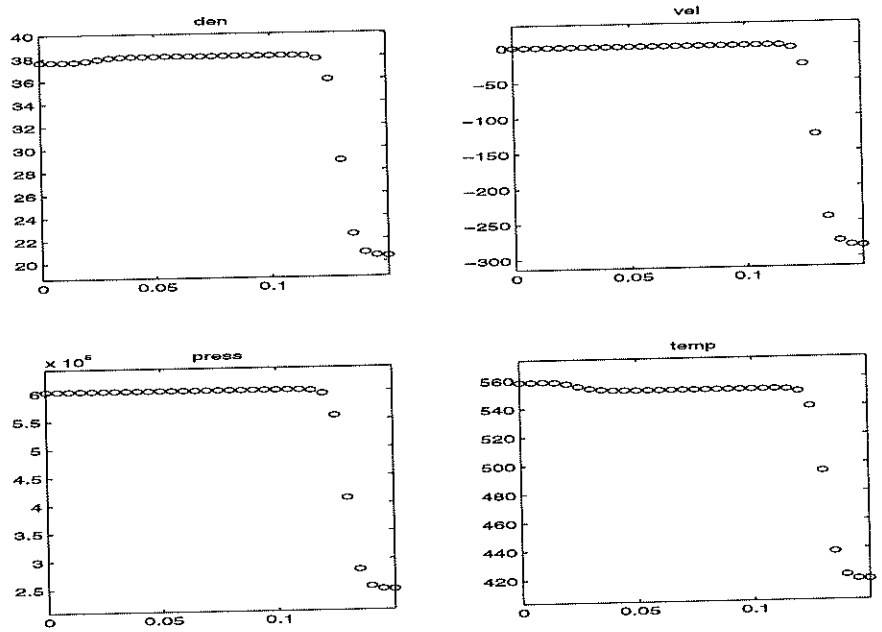

Figure 9: Ideal Gas, ENO-LLF-M, $T'(\rho)$ constant

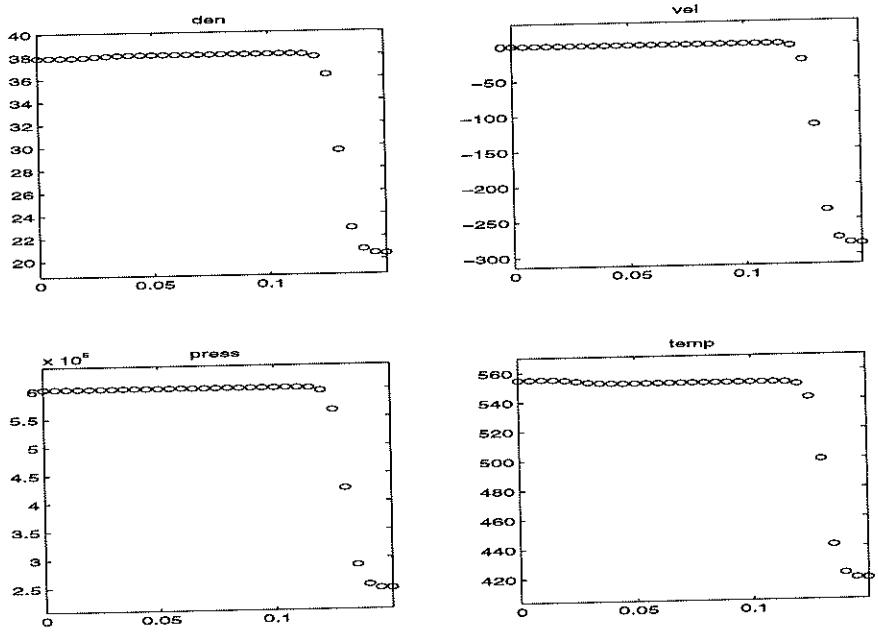

Figure 10: Ideal Gas, ENO-LLF-M, constant entropy

6.2 Example 2

In this example we start the fluid at rest, $u = 0$, and at $T = 300K$. Then the piston (initially located at $0m$) is instantaneously set to a velocity of $1000\frac{m}{s}$ driving to the right. There is no time for the fluid to react to a smoothly accelerated piston. Our acceleration is infinite!

Our first test is with the ideal gas equation of state where we choose the uniform initial density to be $10\frac{kg}{m^3}$. The results are shown in figure 11 for ENO-RF. The results for $T'(\rho)$ constant isobaric fix (equivalent to $e'(\rho)$ constant isobaric fix) are shown in figure 12, while the results for the constant entropy isobaric fix are shown in 13.

Next we try the Marquina style Jacobian evaluation and note it suffers from "underheating" as shown in figure 14 for ENO-LLF-M. In figure 15, we combine ENO-LLF-M with the $T'(\rho)$ constant isobaric fix and note that the isobaric fix improves the "underheating" problem.

For the Tait solid equation of state, we choose the uniform initial density to be $1900\frac{kg}{m^3}$. The results in figure 16 show the "overheating" errors for the ENO-LLF scheme. Figures 17, 18, and 19 show the improvement gained by using any of the three isobaric fixes.

For the virial gas equation of state, we choose the uniform initial density to be $10\frac{kg}{m^3}$. The results in figure 20 show the "overheating" errors for the ENO-RF scheme, while figure 21 shows the results with the $T'(\rho)$ constant isobaric fix (which is equivalent to the $e'(\rho)$ constant isobaric fix for the virial gas equation of state).

In general, the isobaric fix does not completely eliminate the "overheating" errors, but it does limit them to more acceptable levels. In contrast, unfixed schemes can accumulate large errors in density and temperature. In fact, our experiments have shown that some schemes will eventually fail due to nonphysical negative values of either density or temperature.

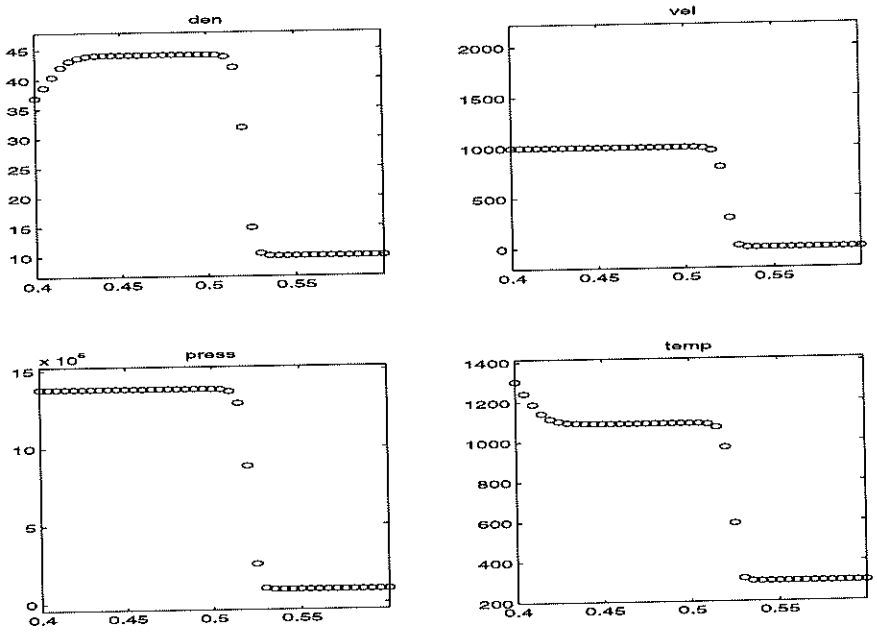

Figure 11: Ideal Gas, ENO-RF, "overheating"

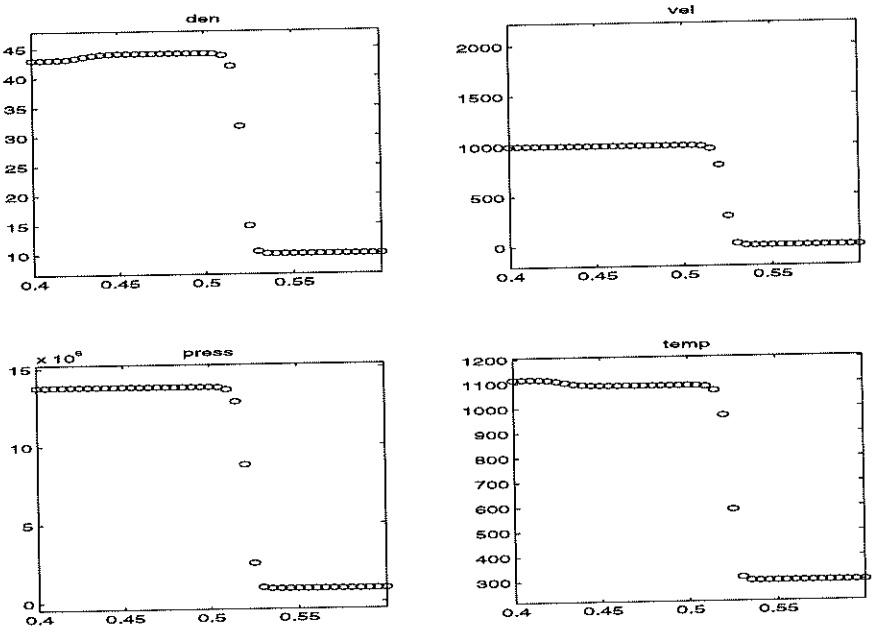

Figure 12: Ideal Gas, ENO-RF, $T'(\rho)$ constant

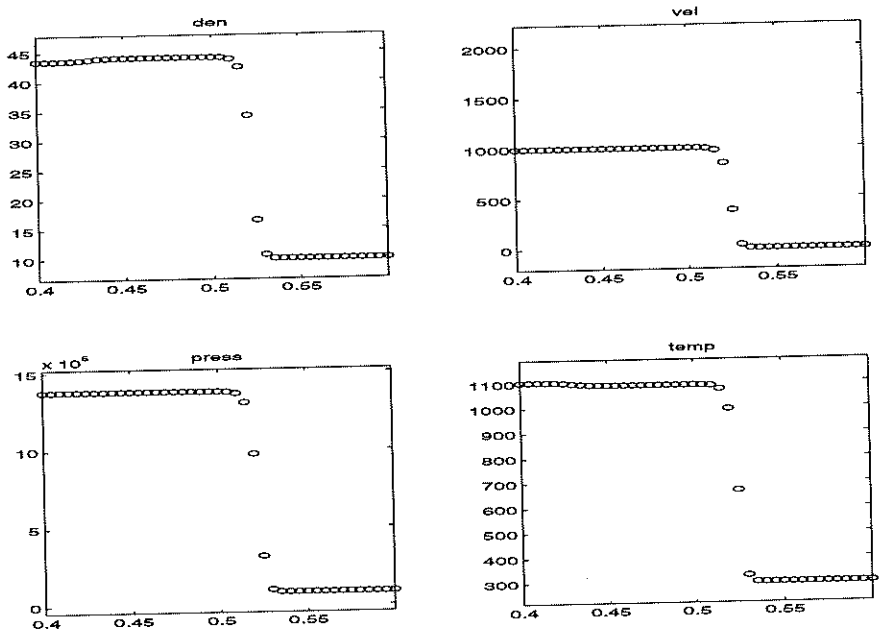

Figure 13: Ideal Gas, ENO-RF, constant entropy

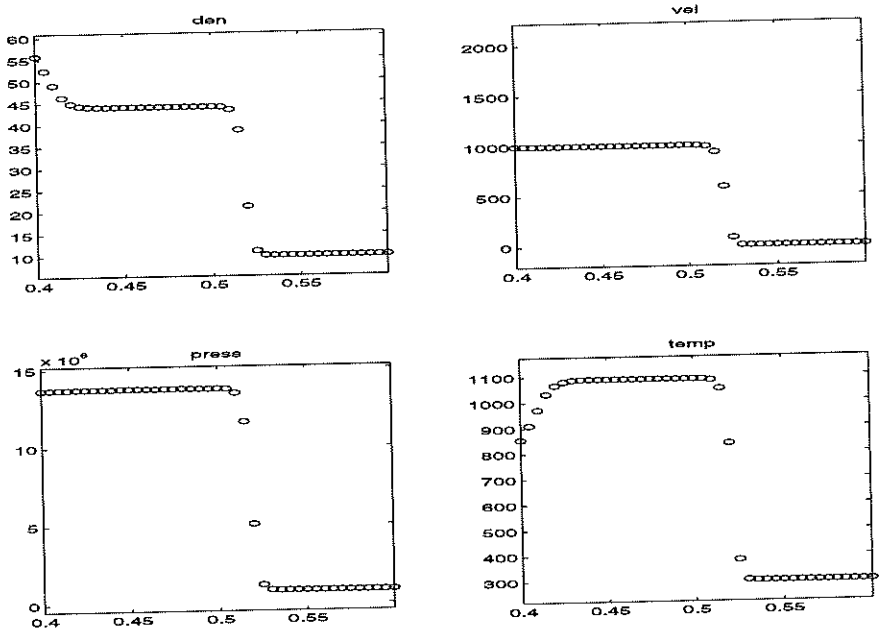

Figure 14: Ideal Gas, ENO-LLF-M, "underheating"

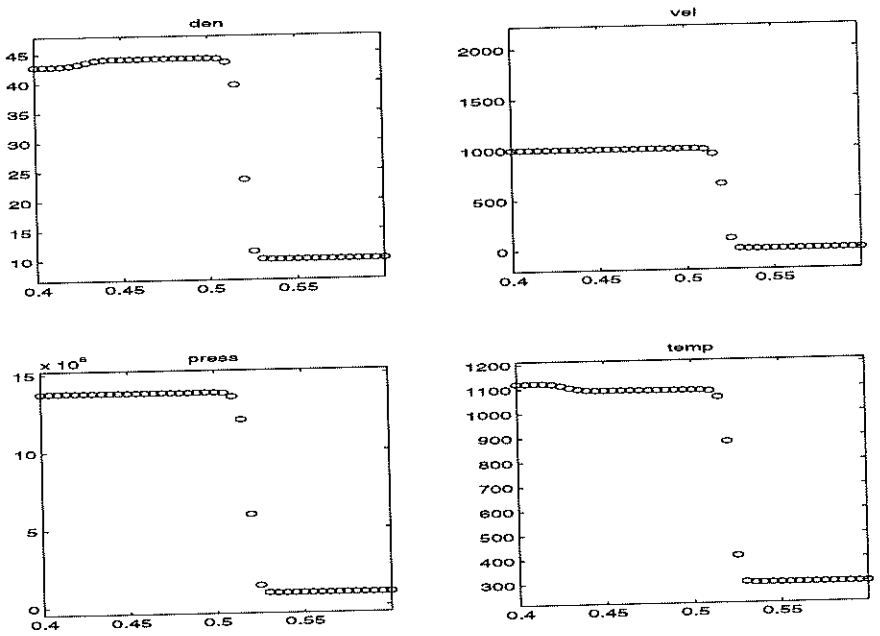

Figure 15: Ideal Gas, ENO-LLF-M, $T'(\rho)$ constant

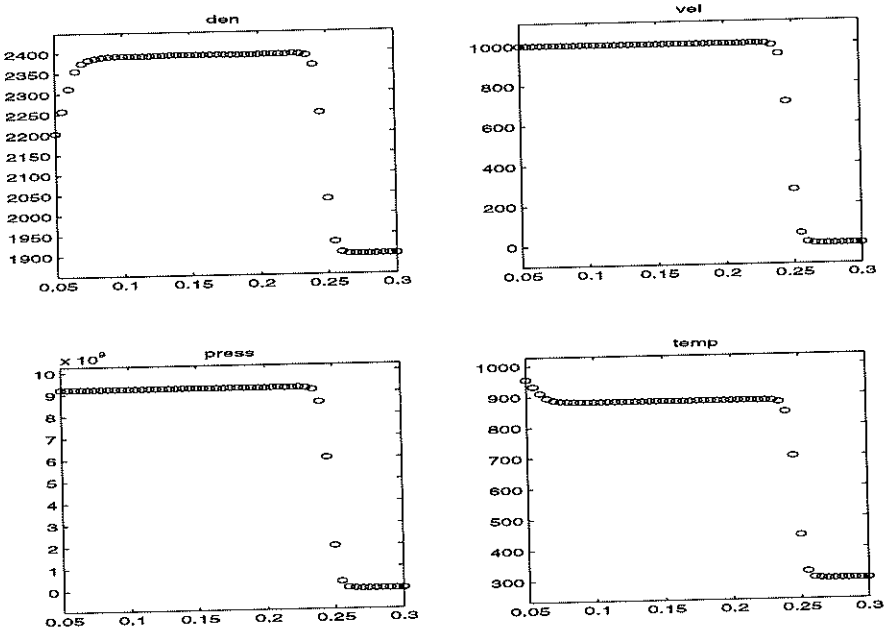

Figure 16: Tait Solid, ENO-LLF, "overheating"

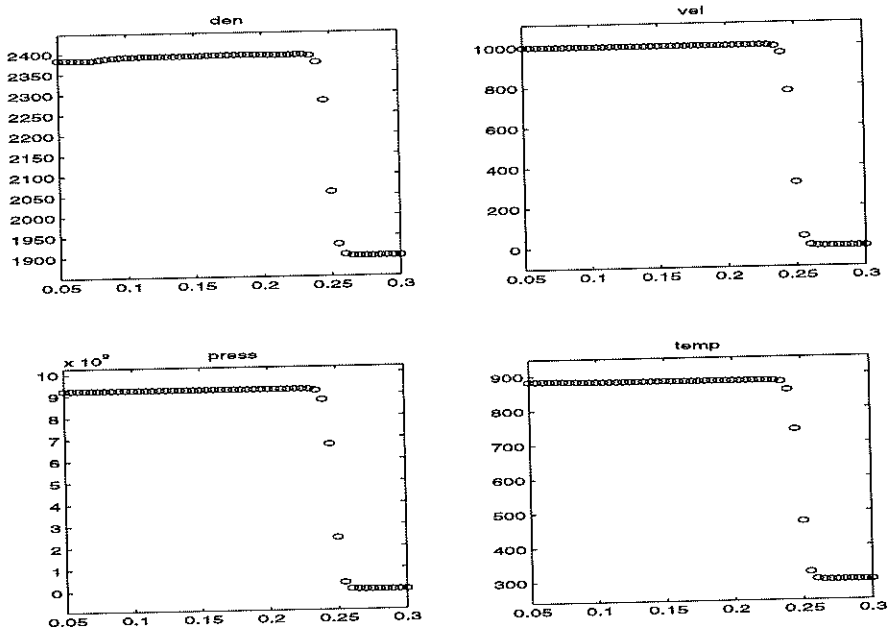

Figure 17: Tait Solid, ENO-LLF, $T'(\rho)$ constant

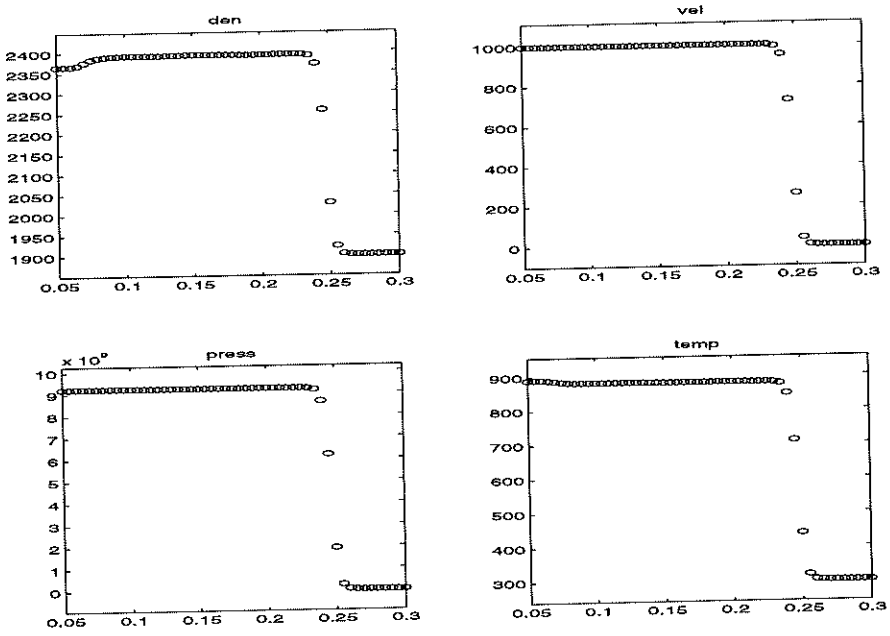

Figure 18: Tait Solid, ENO-LLF, $e'(\rho)$ constant

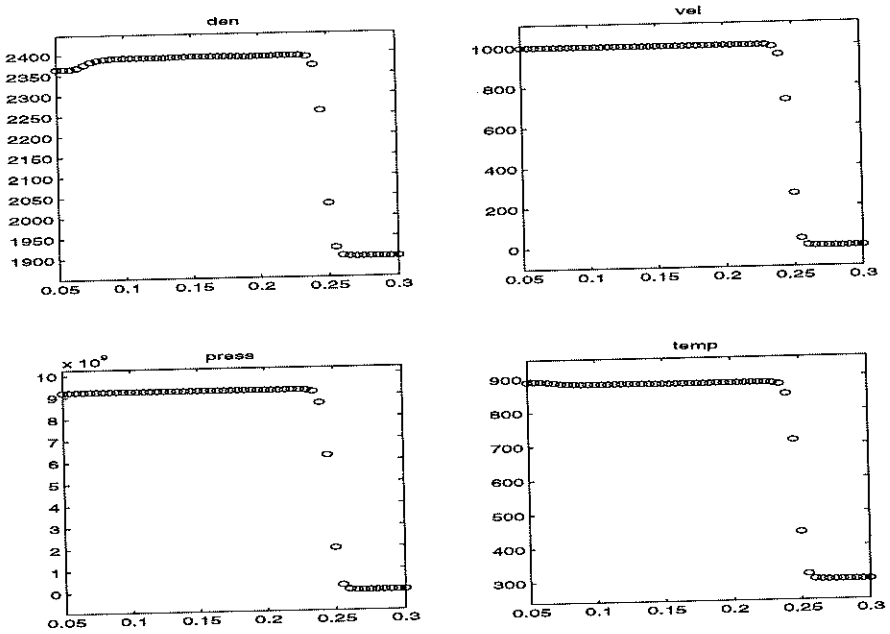

Figure 19: Tait Solid, ENO-LLF, constant entropy

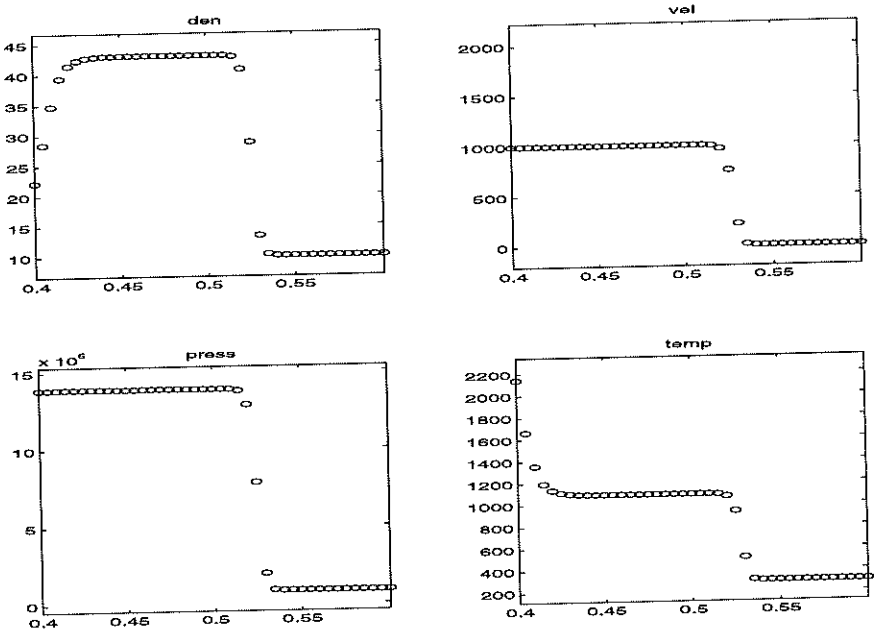

Figure 20: Virial Gas, ENO-RF, "overheating"

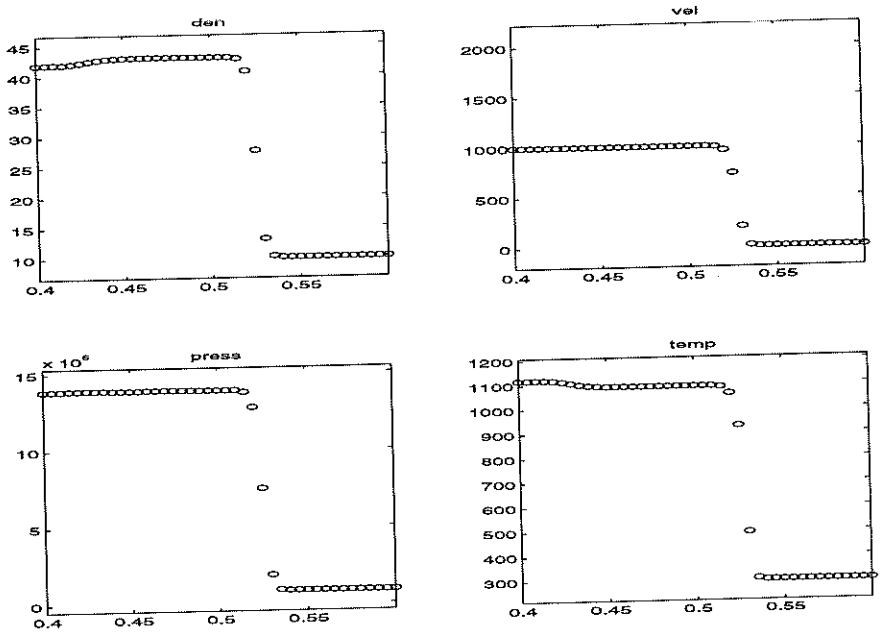

Figure 21: Virial Gas, ENO-RF, $T'(\rho)$ constant

6.3 Example 3

In this example we start the fluid at rest, $u = 0$, and at $T = 300K$. Then the piston (initially located at $.3m$) is instantaneously set to a velocity of $-100\frac{m}{s}$. That is, we instantaneously pull the piston to the left (away from the fluid).

We use the ideal gas equation of state with a uniform initial density of $10\frac{kg}{m^3}$. The results in figure 22 show the "overheating" errors for the ENO-RF scheme, while figure 23 shows the results with the $T'(\rho)$ constant isobaric fix (which is equivalent to the $e'(\rho)$ constant isobaric fix). Figure 24 shows the results with the constant entropy isobaric fix.

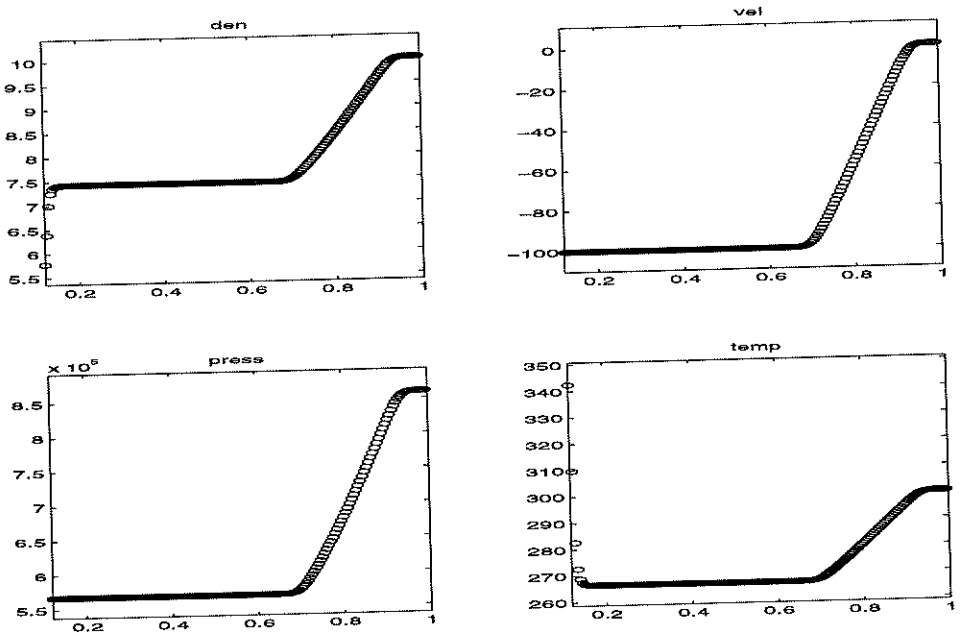

Figure 22: Ideal Gas, ENO-RF, "overheating"

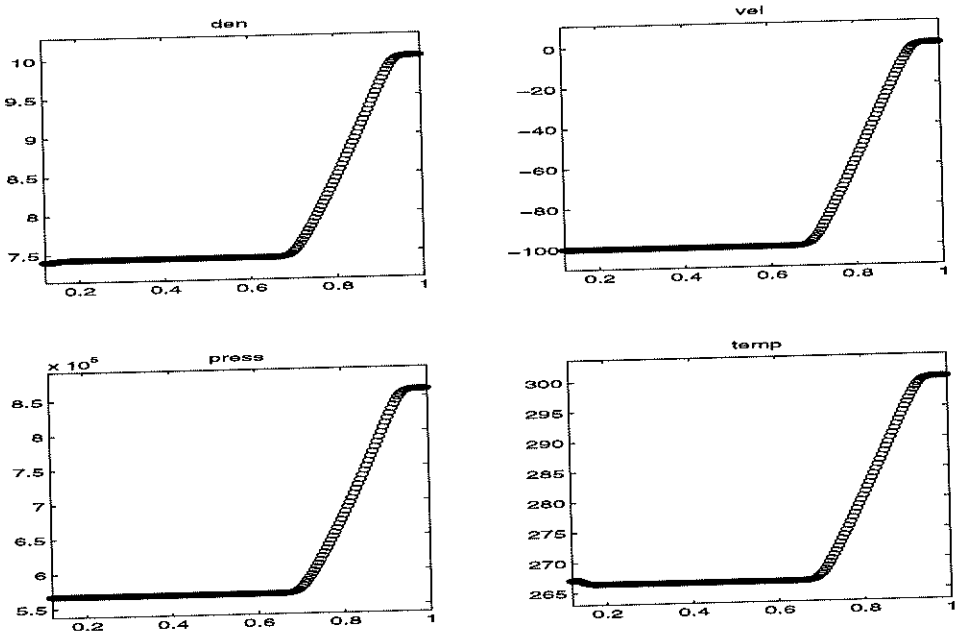

Figure 23: Ideal Gas, ENO-RF, $T'(\rho)$ constant

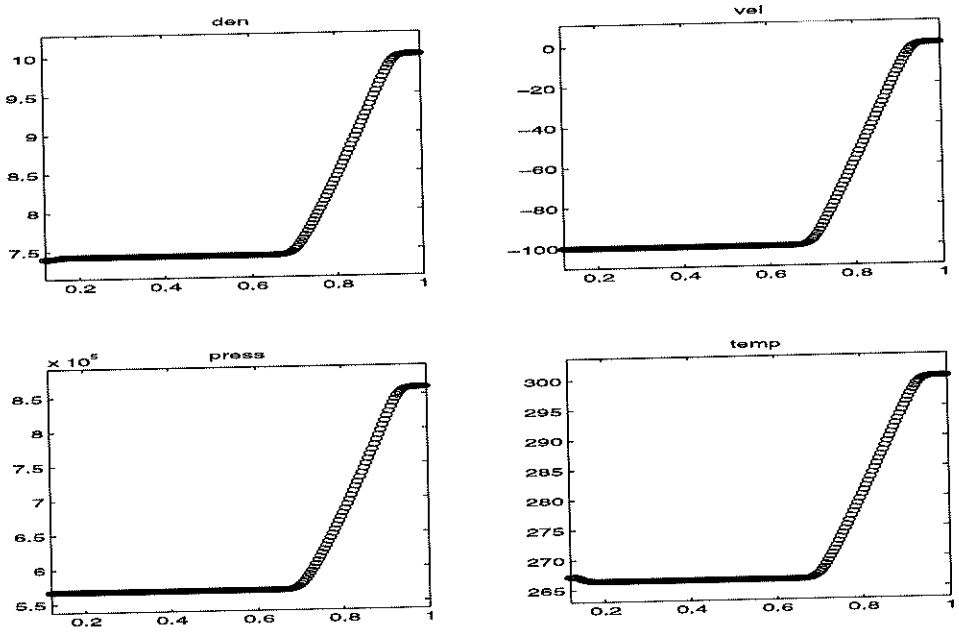

Figure 24: Ideal Gas, ENO-RF, constant entropy

6.4 Example 4

In this example, we consider test cases from [14].

Consider a $1m$ domain with a stationary solid wall boundary located at $0m$. We use 100 grid points with $\gamma = \frac{5}{3}$ and $M = .029\frac{kg}{mol}$ in the ideal gas equation of state. Initially, $\rho = 1$, $u = -1$ and $p = 0$ are defined everywhere on the domain. Note that the wall is placed at a flux, not at a grid point.

Since the sound speed is initially $c = 0$, we use the 2nd order central scheme from [11]. Figure 25 shows the "overheating" errors, and figure 26 shows the improvement with the $T'(\rho)$ constant isobaric fix.

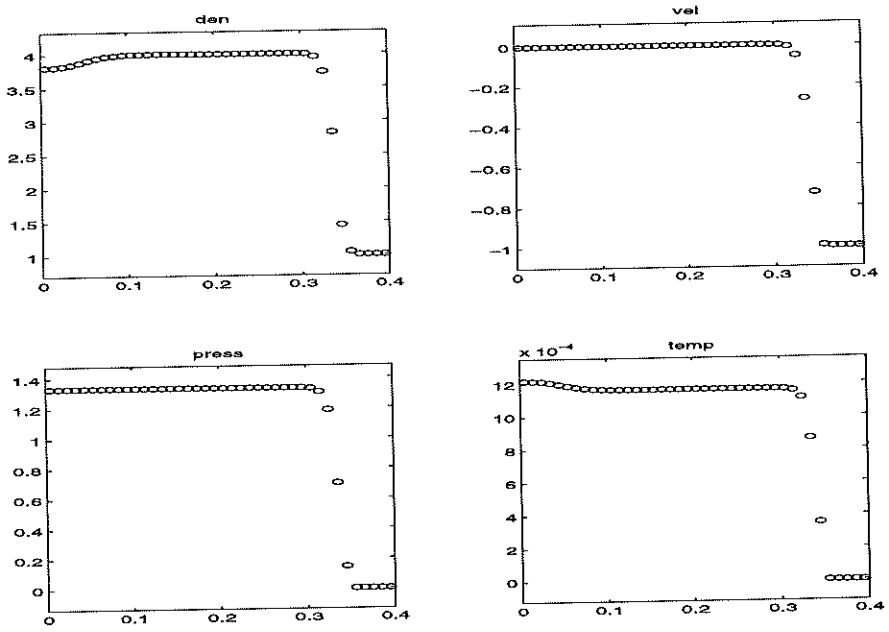

Figure 25: Planar Noh problem, "overheating"

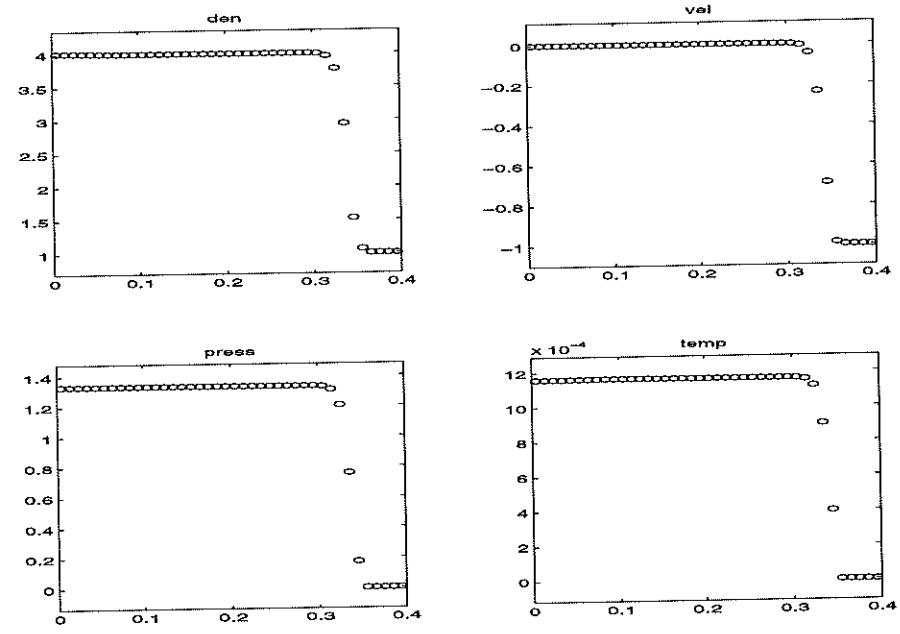

Figure 26: Planar Noh problem, $T'(\rho)$ constant

7 A Two Dimensional Test

In this section we consider the two dimensional Mach 3 step flow test problem [17] where the reflecting boundary conditions are crucial in determining the quality of the numerical approximation. The tunnel is 3 units long and 1 unit wide with a .2 unit high step which is located .6 units from the left hand side of the tunnel. We use a gamma law gas with $\gamma = 1.4$. The initial conditions are $\rho = 1.4$, $p = 1$, $u = 3$, and $v = 0$. An inflow boundary condition is applied at the left end of the computational domain and an outflow boundary condition is applied at the right end. We apply reflecting boundary conditions along the walls of the tunnel.

The density profile is the hardest to compute due to the Mach stem at the upper wall and the contact discontinuity it generates, and due to the corner of the step which is a singularity of the boundary of the domain and the center of a rarefaction fan, i.e. a singular point of the flow. In an attempt to minimize numerical errors generated at the corner of the step, Woodward and Colella propose an additional boundary condition [17] near the corner of the step in order to maintain steady flow around this singular point. They propose two corrections: constant entropy and constant enthalpy to a group of six cells near the corner of the step using an upstream point as a reference. The details of these two corrections are outlined in [3] (in equation 24 of [3], the second appearance of ρ_b should be P_b).

The overheating phenomenon can be observed along all reflecting boundaries of the domain by looking at the level curves near the walls. More orthogonal level curves impinging on the reflecting walls imply less "overheating" errors. We note that the $T'(\rho)$ constant isobaric fix dramatically reduces "overheating" errors, and a direct consequence of this is an additional reduction in other errors such as the "kinked" Mach stem and numerical artifacts related to the "carbuncle phenomenon" (associated with nearly stationary shocks near a reflecting wall). We note that Marquina's flux splitting eliminated these numerical pathologies in [3].

The numerical results shown are on an equally spaced grid with $dx = dy = \frac{1}{40}$ and finer grids showed similar results. We run the code to a final time of $t = 4$ when the flow has a rich and interesting structure which is the "culture medium" for growing numerical errors associated with near stationary shock waves aligned with the grid, and their interaction with reflecting

walls producing large "overheating" errors. In order to be concise we ran all the experiments for the 3rd order PHM reconstruction [12]. Each contour plot in this section displays thirty equally spaced level curves between the minimum and maximum values of the computed density.

In this first example, we use the standard Jacobian technique as opposed to Marquina's flux splitting. In addition we use the standard six cell enthalpy and entropy correction. In the top plot of figure 27 we display numerical approximations of the flow density for PHM-RF (the 'RF' notation is described in [16]) where the "kinked" Mach stem is conspicuous. The middle plot was obtained with the same algorithm with the $T'(\rho)$ constant isobaric fix correction applied along the solid walls using the third cell from the wall to correct the second cell from the wall and then that cell to correct the cell adjacent to the wall. (we find this double correction satisfactory for high order resolution). The bottom plot represents the numerical approximation obtained with the more viscous PHM-LLF (the LLF notation is described in [16]). While both the isobaric fix and the more viscous PHM-LLF method removed the "kinked" Mach stem pathology, the isobaric fix has the advantage of a much sharper contact discontinuity. In figure 28 we display the corresponding $y = .2$ section of the adiabatic exponent to see how entropy is preserved at the corner of the step.

In this example we use PHM-RF-M (where the 'M' denotes the application of Marquina's flux splitting technique as opposed to the standard Jacobian evaluation). In the top plot of figure 27, we used the standard corner treatment. The middle plot uses the standard corner treatment with the $T'(\rho)$ constant isobaric fix along reflecting walls. The bottom plot was obtained by applying the isobaric fix with constant $T'(\rho)$ along reflecting walls and only an enthalpy correction at the corner, i.e. no entropy correction at the corner. Note that the bottom numerical approximation gives an accurate prediction of the shock wave location without the entropy fix! This is the only method we know of that can predict the shock wave location without the entropy fix. In figure 30 we observe the entropy preservation at the corner for the corresponding numerical approximations that appear in figure 29.

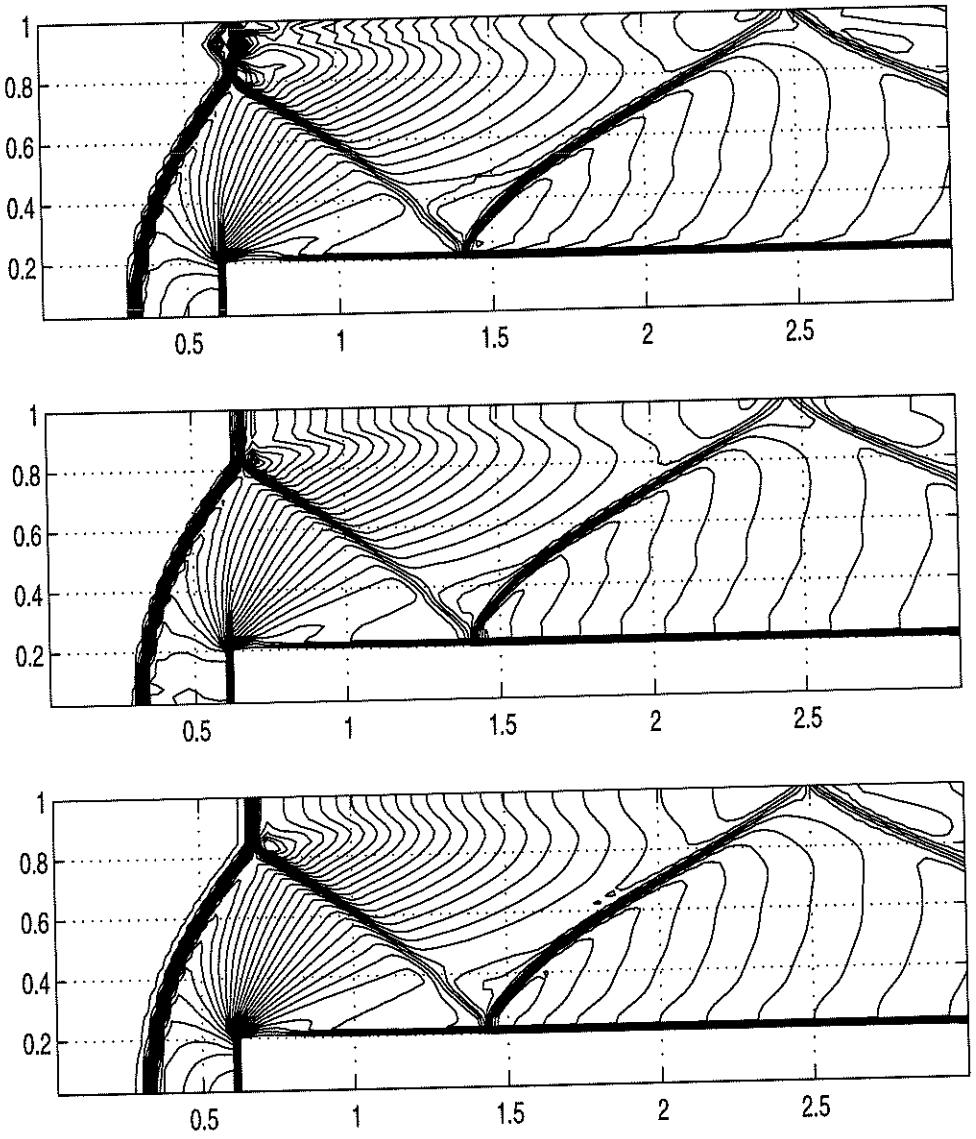

Figure 27: Contour plots of numerical approximations to the density: PHM-RF (top), PHM-RF with constant $T'(\rho)$ isobaric fix (middle), PHM-LLF (bottom).

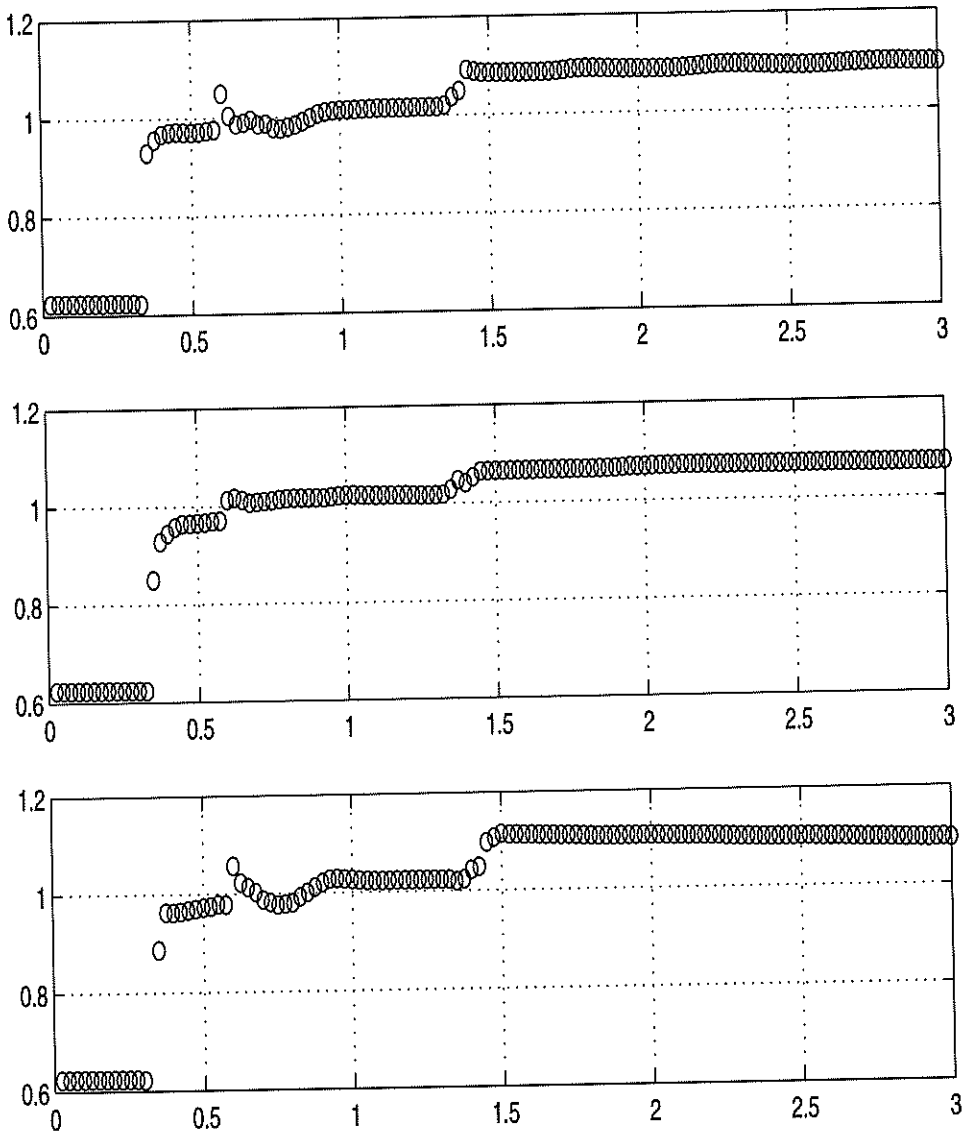

Figure 28: Adiabatic Exponents for the previous figure (one dimensional y-sections at y=.2).

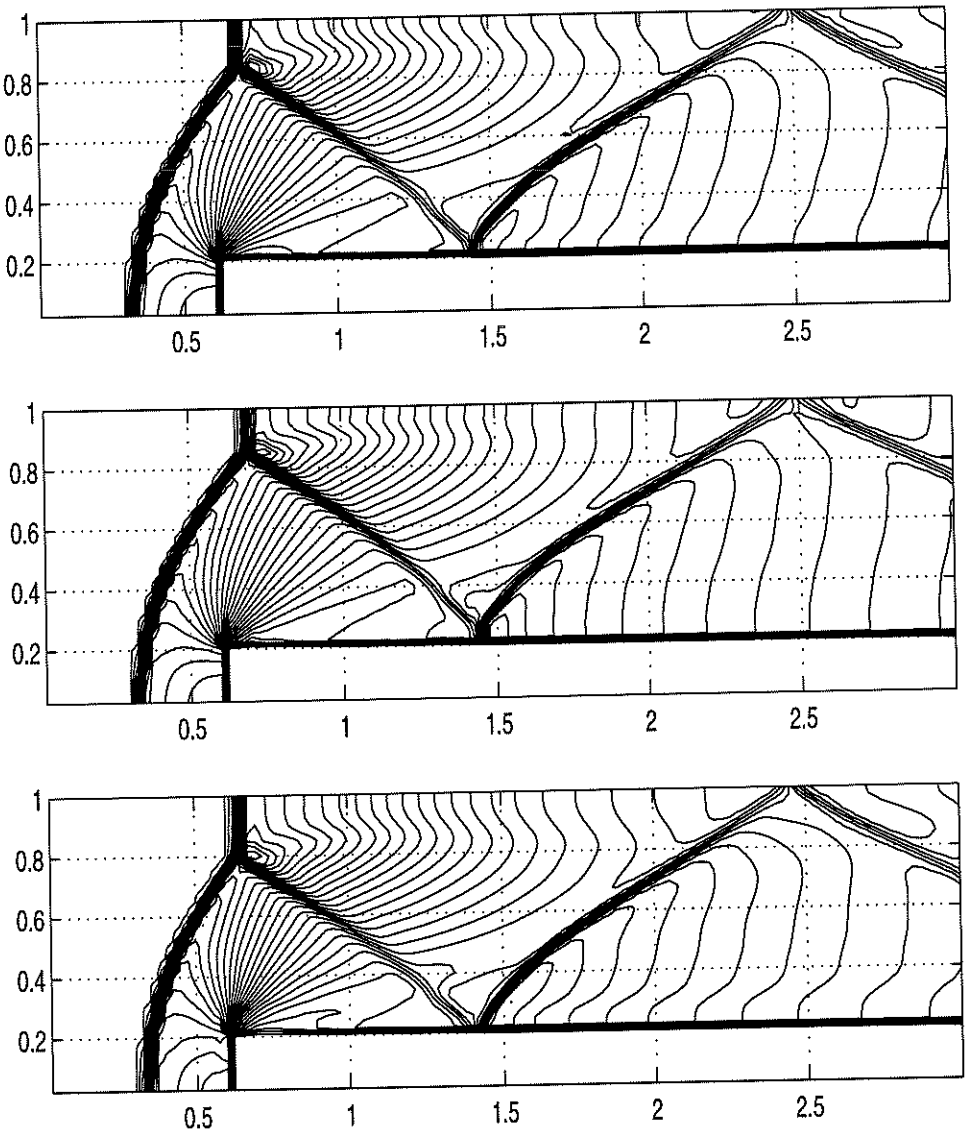

Figure 29: Contour plots of numerical approximations to the density with PHM-RF-M: standard corner treatment (top), standard corner treatment with $T'(\rho)$ constant isobaric fix (middle), no entropy correction with $T'(\rho)$ constant isobaric fix (bottom).

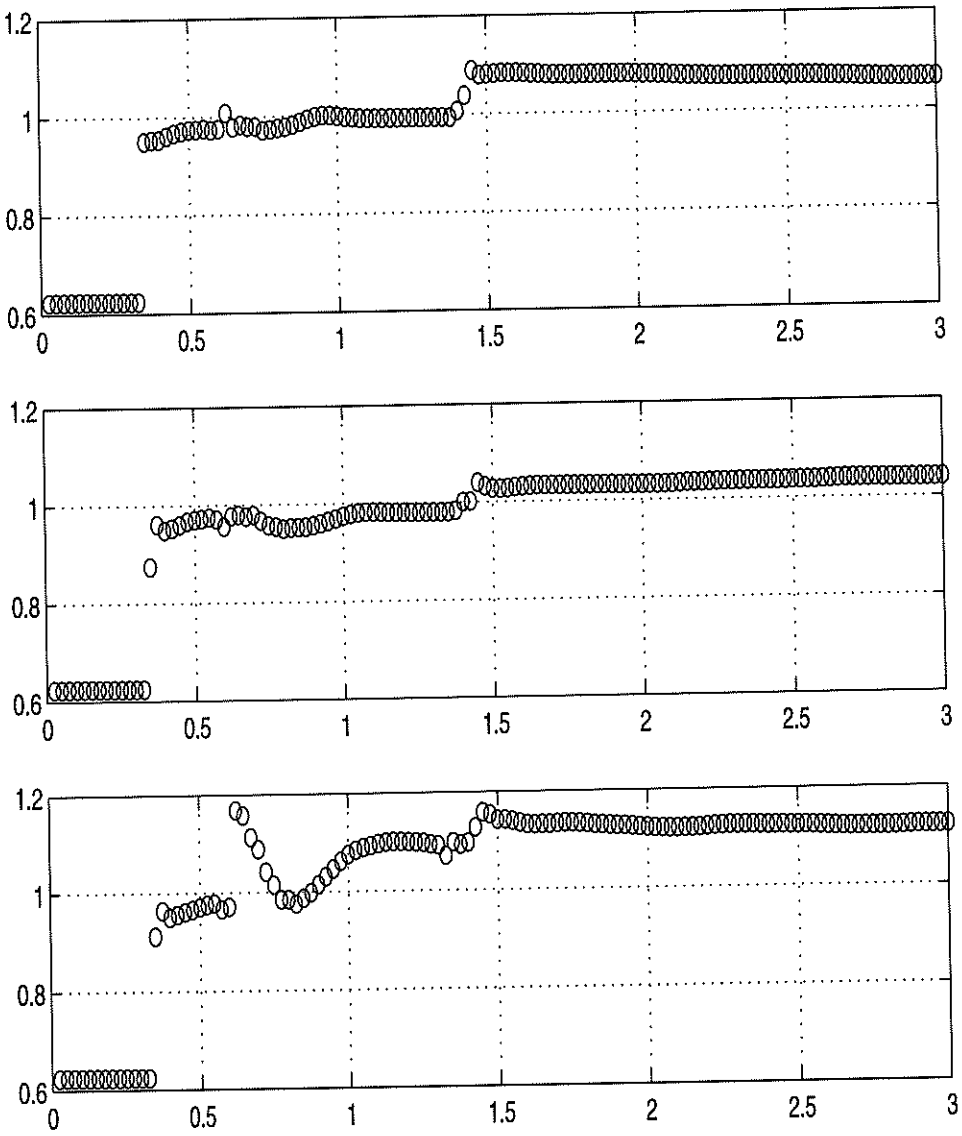

Figure 30: Adiabatic Exponents for the previous figure (one dimensional y-sections at y=.2).

References

[1] Atkins, P., *Physical Chemistry*, 5th edition, Freeman, 1994.

[2] Atkinson, Kendall E., *An Introduction to Numerical Analysis*, Wiley, 1989.

[3] Donat, R. and Marquina, A. *Capturing Shock Reflections: An Improved Flux Formula*, J. Computational Physics, vol 125, 42-58 (1996).

[4] Fedkiw, R., Merriman, B., Donat, R., and Osher, S., *The Penultimate Scheme for Systems of Conservation Laws: Finite Difference ENO with Marquina's Flux Splitting*, UCLA CAM Report 96-18, July 1996, http://www.math.ucla.edu/applied/cam/.

[5] Fedkiw, R., Merriman, B., and Osher, S., *Efficient characteristic projection in upwind difference schemes for hyperbolic systems (The Complementary Projection Method)*, J. Computational Physics, vol. 141, 22-36 (1998).

[6] Fedkiw, R., Merriman, B., and Osher, S., *High accuracy numerical methods for thermally perfect gas flows with chemistry*, J. Computational Physics 132, 175-190 (1997).

[7] Glaister, P., *An Approximate Linearised Riemann Solver for the Euler Equations for Real Gases*, J. Computational Physics 74, 382-408 (1988).

[8] Gonthier, Keith Alan, *A Numerical Investigation of the Evolution of Self-Propagating Detonation in Energetic Granular Solids*, University of Notre Dame (Dissertation), 1996.

[9] Hirsch, C., *Numerical Computation of Internal and External Flows*, Volume 2, Wiley 1990.

[10] G.-S. Jiang and C.-W. Shu, *Efficient Implementation of Weighted ENO Schemes*, J. Computational Physics, v126, 202-228, (1996).

[11] Liu, X-D., and S. Osher, *Convex ENO High Order Schemes Without Field-by-Field Decomposition or Staggered Grids*, J. Comput Phys, v142, pp 304-330, (1998).

[12] Marquina, A., *Local Piecewise Hyperbolic Reconstruction of Numerical Fluxes for Nonlinear Scalar Conservation Laws*, SIAM J. Sci. Comput., vol 15, pp. 892 (1994).

[13] Menikoff, R., *Errors When Shock Waves Interact Due to Numerical Shock Width*, SIAM J. Sci. Comput., v15, n5, 1227-1242 (1994).

[14] Noh, W., *Errors for Calculations of Strong Shocks Using an Artificial Viscosity and an Artificial Heat Flux*, J. Computational Physics 72, 78-120, (1978).

[15] Sanders, R. and Weiser, A., *High Resolution Staggered Mesh Approach for Nonlinear Hyperbolic Systems of Conservation Laws*, Journal of Computational Physics, 101, 314-329 (1992).

[16] Shu, C.W. and Osher, S., *Efficient Implementation of Essentially Non-Oscillatory Shock Capturing Schemes II (two)*, Journal of Computational Physics; Volume 83, (1989), pp 32-78.

[17] Woodward, P. and Colella, P. *The Numerical Simulation of Two-Dimensional Fluid Flow with Strong Shocks*, J. Computational Physics, 54, 115-173 (1984).